METHODOLOGY FOR ANALYSIS OF TRAFFIC-INDUCED BUILDING VIBRATIONS

RICKARD TORNDAHL and TOBIAS SVENSSON

Structural Mechanics

Master's Dissertation

METHODOLOGY FOR ANALYSIS OF TRAFFIC-INDUCED BUILDING VIBRATIONS

RICKARD TORNDAHL and TOBIAS SVENSSON

Abstract

Urban population growth leads to denser cities where buildings are being constructed closer to sources of vibration like motorways, railways and tramways. The risk of disturbing vibrations is thereby increasing which could affect residents and sensitive equipment, for instance equipment used in hospitals. In the Master's thesis, the effect of structural design on traffic-induced building vibrations has been studied.

A methodology was developed and numerical simulations were carried out using the finite element (FE) method. The methodology holds two parts, one part where a large FE model of the ground is reduced and one part where a parameter study is conducted. In the reduction part, the FE ground model is established and a dynamic condensation is performed which results in a reduced ground model. In the parameter study part of the developed methodology, a FE building model is created and a dynamic stiffness matrix for each studied frequency is determined. The dynamic stiffness matrix of the building model is assembled with the dynamic stiffness matrix of the reduced FE ground model and analyses are conducted. This allows for changes to be made in the building model and new analyses to be performed without the need to implement the large non-reduced ground model. The computational time to perform the parameter study was thereby decreased by 99.7% compared to using the non-reduced FE ground model.

The parameter study was performed by steady-state analyses in the frequencies interval of 5–50 Hz with 1 Hz steps. A unit load was applied at a distance of 20 m from a reference building. The results from the parameter study showed that structural design can influence the response of the building significantly. The eigenfrequencies of the building are of importance and a coinciding frequency between the load and the eigenfrequency of the building resulted in a peak response of the vibration level inside the building.

The work made in the thesis contributes in the ambition towards enabling predictions of vibrations by use of numerical models. As the developed methodology in the thesis can make numerical simulations more efficient in a way that less computational time and less computational resources are needed.

Keyword: Traffic-induced vibration, finite element method, dynamic reduction, wave propagation, structural dynamics, soil dynamics, infinite elements, building vibration, structural design

Preface

This Master's thesis concludes our five years of studies at the Faculty of Engineering, Lund University. The work was performed at the Division of Structural Mechanics.

We would like to thank Prof. Kent Persson and our supervisor Dr. Peter Persson for providing the initial idea of the thesis and being active in the discussions concerning our work. We are also grateful to M.Sc. Jens Malmborg for providing guidance with the finite element software Abaqus. Also, thanks to the staff at the Division of Structural Mechanics for an inviting atmosphere and being part of rewarding discussions concerning both our work and theirs.

I would like to direct many thanks to my family and friends for their support throughout my life - and in particular my father Jörgen, my mother Eva, my brother Fredrik and my sister Cajsa.

I would like to thank my family and friends for supporting me throughout life. Especially my parents Lena and Michael, my sisters Julia and Martina and my girlfriend Lovisa Nilsson.

Tobias Svensson, Lund, June 2017

Rickard Torndahl, Lund, June 2017

Nomenclature

Roman symbols

P-wave	Pressure wave
R-wave	Rayleigh wave
S-wave	Shear wave
V, H	Vertical and Horizontal complex velocity amplitude, respectively
r, e	Subindex, denoting retained and eliminated dofs
c	Viscous damping constant
c_S	Shear wave velocity
c_P	Pressure wave velocity
c_R	Rayleigh wave velocity
d_P, d_S	Dashpot damping coefficients
E	Young's modulus
E_D	Dissipated energy in one cycle of harmonic vibration
E_S	Strain energy
f	Frequency
$f(t)$	Time-dependent force
i	Imaginary unit
k	Stiffness
m	Mass
t	Time
u	Displacement
$\dot{u}$	Velocity
$\ddot{u}$	Acceleration
v	Poisson's ratio

Roman bold symbols

$\mathbf{C}$	Damping matrix
$\mathbf{C_S}$	Structural damping matrix
$\mathbf{C_V}$	Viscous damping matrix
$\mathbf{D}$	Dynamic stiffness matrix
$\mathbf{\tilde{D}}$	Reduced dynamic stiffness matrix
$\mathbf{f}$	External force vector
$\mathbf{I}$	Identity matrix
$\mathbf{K}$	Stiffness Matrix
$\mathbf{L}, \mathbf{U}$	Lower and upper triangular matrix, respectively
$\mathbf{M}$	Mass Matrix
$\mathbf{u}$	Displacement vector
$\mathbf{\dot{u}}$	Velocity vector
$\mathbf{\ddot{u}}$	Acceleration vector

Greek symbols

η	Loss factor
λ	Lamé constant
Λ	Wave length
μ	Lamé constant (Also known as the shear modulus)
ρ	Density
$\mathbf{\Phi}$	Eigenmode vector of a system
ω	Angular frequency

Contents

1 Introduction

1.1 Background

More than half of the world's population lives in cities and the UN predicts that the number of people living in urban areas will increase by 1.5 billion in the next 15 years [1]. As the population size in cities grows, more facilities are needed, such as housing, subway stations and industrial buildings. These facilities are being constructed at the unbuilt spaces within the cities, often closer to sources of vibrations such as motorways, railways and tramways. In addition, construction of new transportation systems closer to existing buildings are conducted. This increases the risk of disturbing vibrations, which could affect residents and sensitive equipment, for instance equipment used in hospitals [2]. It is thus important to develop vibration-reduction methods to meet the need of denser cities.

Today, methods such as digging a trench or creating barriers, e.g. sheet piles or buried walls, are common vibration-reduction measures. It is also known that the vibration level within buildings are effected by the type of building. For example, the vibration level in a building might be different in a heavy-weight building compared to a light-weight building. If more knowledge were available about how different design choices of a building effect the vibrations, the construction industry could apply these in the early planning stage as a reduction measure. The vibration level within buildings needs to be predicted in order to evaluate the effectiveness of vibration-reduction measures. The construction industry is consequently in need of both better knowledge and tools to predict and analyse building vibrations.

1.2 Aim and objective

The aim of the Master's thesis is to obtain more knowledge of building vibrations induced by traffic and the effect structural design might have on these vibrations. By understanding the effect structural design have on traffic-induced building vibrations, design choices could be made in the early planning stage of a buildings construction to reduce and avoid disturbing vibrations. The objective of the Master's thesis is to develop a methodology for analysing and predicting traffic-induced building vibrations that, in the long term, could be used by the building industry.

1.3 Method

The study has been performed numerically using the finite element method. The methodology used in the thesis was developed together with Prof. Kent Persson and the study was advised by Dr. Peter Persson. Comparative and conceptual studies were the key issue and concern of the Master's thesis.

1.4   Outline

- Chapter 1 contains background, aim and objective, method and the outline of the Master's thesis.

- Chapter 2 gives an overview of vibration transmission from source to receiver. Wave propagation in ground is described, where different wave types are introduced and their properties are described.

- Chapter 3 contains the governing theory.

- Chapter 4 describes the developed methodology. The reduction of the ground model and the procedure of a parameter study are described.

- Chapter 5 describes the ground model and presents the convergence studies of which the ground model's geometry and mesh size are dependent on.

- Chapter 6 presents the results from the parameter study. The reference building that was used is also presented here.

- Chapter 7 contains concluding remarks of the Master's thesis.

2 Traffic-induced vibrations

Vibrations in a built environment can have both natural and man-made origin. Explosions, constructions and traffic are examples of man-made activities that generate vibrations, in contrast to earthquakes and other seismic activities which are natural events. The study of vibrations induced by traffic has become more important in recent years because of the increased awareness of the health issues associated with vibrations combined with the increased construction of new facilities closer to sources of vibration such as roadways and train tracks.

The present chapter details some fundamental theory of vibrations that originate from traffic and a description of the transmission process is given. In addition, numerical models to predict vibrations are discussed.

2.1   Transmission

Traffic-induced vibrations can be divided into three parts: the *source* where the vibrations are generated, the *medium* in which the vibrations propagate, and the *receiver*. Knowledge of these three parts is important to be able to analyse and predict vibration levels inside buildings. Accurate predictions allows effective vibration-reduction measures to be employed. The transmission process is illustrated in Figure 2.1.
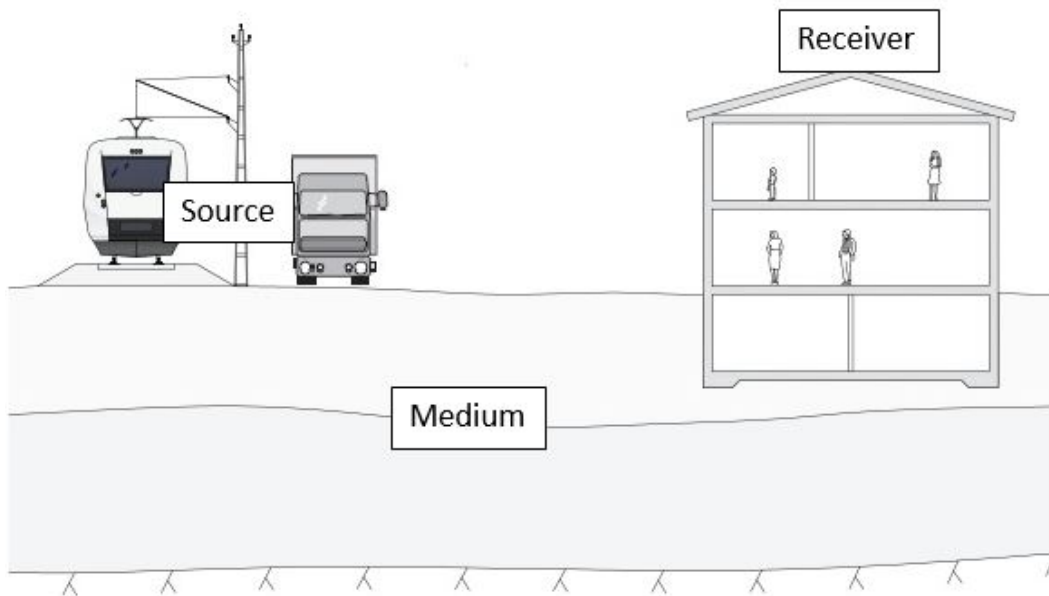
Figure 2.1: *Sketch of vibration-transmission process. Figure source: [3].*

2.1.1   Source

Vibrations originating from traffic sources such as cars, trucks, trains or trams are denoted as traffic-induced vibrations. A vehicle moving at a certain speed will cause a downward deflection of the road or the track on which the vehicle travels. Thus the deflection at a fixed point will be time varying and act as a dynamic excitation, it is by itself a source of vibration but in reality there are other excitation mechanism that also influence the generation of vibrations. Irregularities in the asphalt layer, roughness of rails, or traffic entering and exiting a bridge are examples of such mechanisms. The speed and the weight of the moving vehicle can have a large effect of the generated vibration levels. For example, a high-speed train may travel faster than the generated vibration's wave speed, which will trigger a phenomenon that is similar to sonic booms caused by aeroplanes and a large increase of the generated vibration levels are then expected [4].

Different types of traffic generate vibrations where the amplitude varies with the frequency. It means that the frequencies of interest are different for cars than for trains. For cars and trucks, the highest frequency of interest is usually less than 25 Hz [5] and for trams, the highest frequency of interest is up to approximately 60 Hz [2]. For railway traffic, the highest energy content is usually below 20 Hz [6].

2.1.2   Medium

The generated vibrations propagate through a medium and the dynamic properties of the medium may have great influence on the propagation process. Examples of mediums for traffic sources are tunnels, bridges and the ground. The ground is often stratified with one or more layers of soil on top of bedrock. Also great discontinuities are often present. The properties of the soil layers and the bedrock effect the response of the ground. Depending on the distance between the source and the receiver, the depth of the bedrock surface can also be of great interest. Wave propagation in ground is further described in Section 2.2.

2.1.3   Receiver

The receiver of the vibrations are an object and in a built environment, usually a building. A buildings response to traffic-induced vibrations depends on numerous factors, such as the construction material and the design of the building. Even the placement of furniture within the building can have an effect. Measurements presented by Dawn in [7] indicates that a dynamic amplification can occur, i.e. the building response is larger than the underlying ground response.

Often a maximum allowed vibration level is set for the building. The limitation can be set due to sensitive equipment or instruments to work to its full potential. The limitations can also be set due to human comfort, where the vibrations can cause annoyance. Figure 2.2 shows an approximation of the human perception threshold, as well as the range of moderate and probable disturbance. The sensitivity of human perception differ with frequency where low frequencies, below 8 Hz, are less critical.
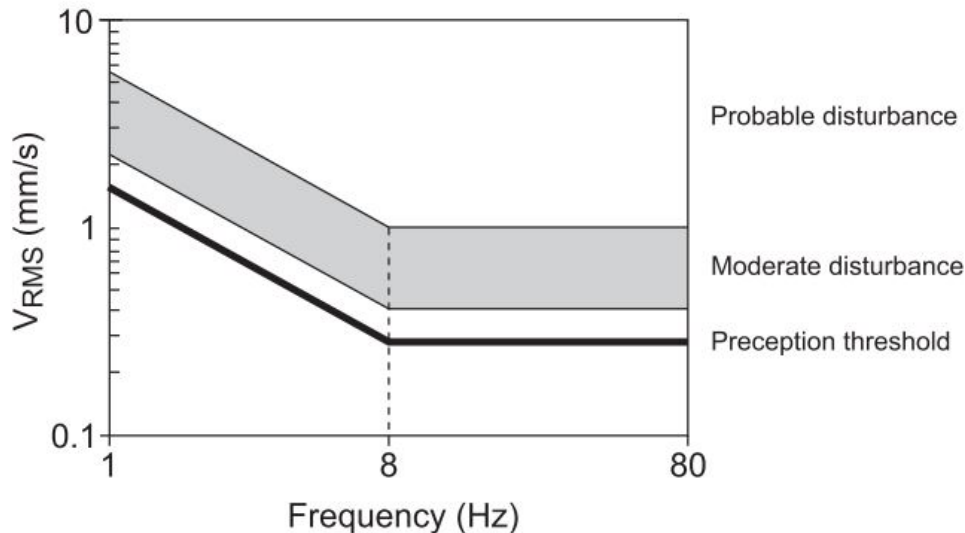
Figure 2.2: *Perception threshold, moderate and probable disturbance ranges [8]. Figure source: [2].*

Regulations

Swedish national regulations provides guidelines for the levels of traffic-induced vibration in buildings. The Swedish Transport Administration, *Trafikverket*, states that no one should be exposed to vibration levels above 0.4 mm/s (RMS value, see Section 3.4) in residential housing [9].

2.2 Wave propagation in ground

Geometrically, the ground is a half-space which means that it expands in the three dimensional (3D) space and is limited by a surface. The ground is often layered with one or more layers of soil on top of bedrock and the wave propagation is highly dependent on the different layers' composition and geometry.

2.2.1 Wave types

In soils, there are body wave motion and surface wave motion that are of interests. As body waves, there are pressure waves (P-waves) and shear waves (S-waves). In P-waves, the particles move parallel to the wave propagation and give rise to compressed and stretched areas in the soil, this is illustrated in Figure 2.3a. In S-waves, the particles move perpendicular to the wave propagation, which is seen in Figure 2.3b. The surface waves that is of interest in this application is the Rayleigh waves (R-waves) which consist of both shear and pressure. The R-waves are categorised as surface waves as they propagate close to the surface of the medium as seen in Figure 2.3c.

(a) *Pressure wave*

(b) *Shear waves*

(c) *Rayleigh waves*
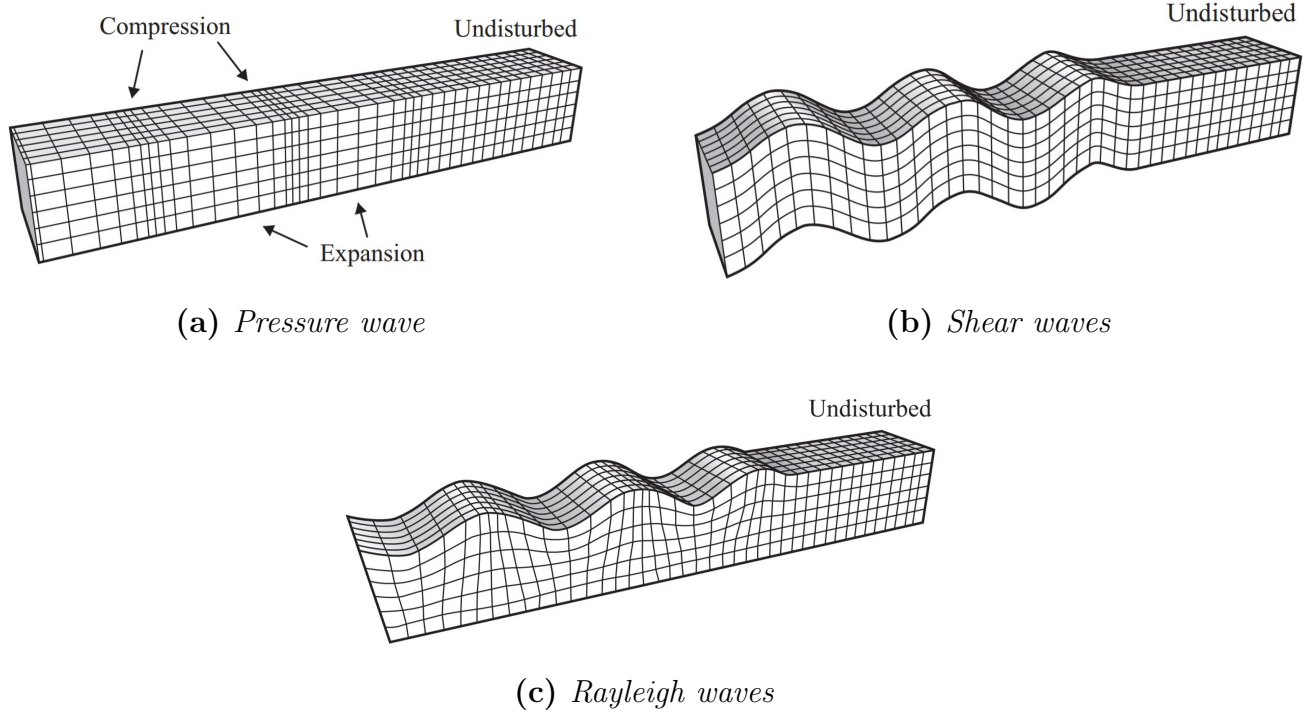
Figure 2.3: *Propagation of three wave types that are of interest in soil in the present application. Figure source: [2].*

The wave velocity depends on the material parameters of the medium in which the wave travel. The velocity of S-waves and P-waves can be calculated as

$$c_S = \sqrt{\frac{\mu}{\rho}} \quad \text{and} \quad c_P = \sqrt{\frac{\lambda + 2\mu}{\rho}}, \tag{2.1}$$

where ρ is the density and μ and λ are the so called *Lamé* constants. These constants are related to the Young's modulus, E, and the Poisson's ratio, v, as

$$\mu = \frac{E}{2(1+v)} \quad \text{and} \quad \lambda = \frac{vE}{(1+v)(1-2v)}. \tag{2.2}$$

It can be observed that the Lamé constant, μ, also is known as the shear modulus. The velocity of Rayleigh waves, c_R, are dependent on several factors, e.g. the Poisson's ratio of the medium. Ground materials, as soil and bedrock can have a Poisson's ratio close to 0.5, the Rayleigh wave velocity can then be related to the velocity of shear waves as, $c_R \approx 0.95c_S$ [10].

The propagation velocity is related to the frequency and the wavelength e.g. the shear wave velocity is related as

$$c_S = f\Lambda_S, \tag{2.3}$$

where f is the frequency and Λ_S is the wavelength of a S-wave.

2.2.2 Geometrical propagation

From a point source, S-waves and P-waves propagate over the volume and form spherical wave fronts. Rayleigh waves are bound to the surface and spreads like "rings on the water" [10]. The propagation of the waves are illustrated in Figure 2.4.

The amplitude of the vibrations tend to decay the further the wave front is from the source. This is partly because the wave energy spreads over a larger area when the distance from the source increases. Body waves decay faster than surface waves as because of the spreading of energy over the volume. Therefore, if the distance is large between the source and the receiver the Rayleigh waves are more important than body waves. In addition, the majority of the energy transmitted to the ground by a surface source leads to the generation of Rayleigh waves [10].

When an incoming wave hit a common boundary between two layers, e.g. a boundary between two soil layers, a part of the wave will be reflected back into the layer it came from. A part of the wave energy will propagate into the adjacent layer, often with a change in the direction of travel. The two phenomena is known as reflection and refraction and are illustrated in Figure 2.5. This indicates that vibrations may not always travel using the shortest path to the receiver.
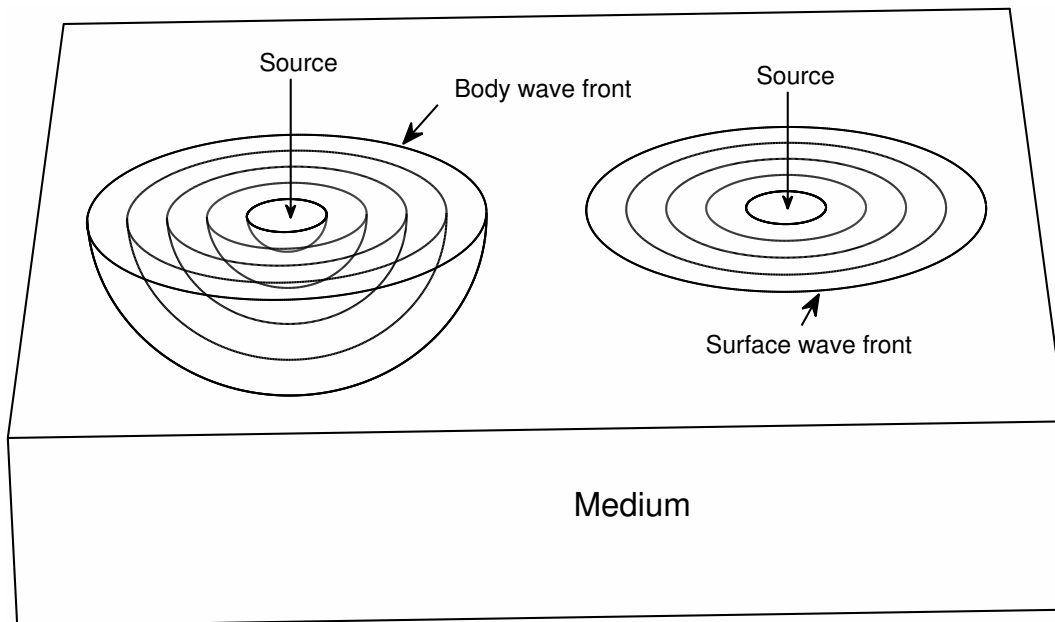
Figure 2.4: *Propagation of body and surface waves in a 3D medium.*
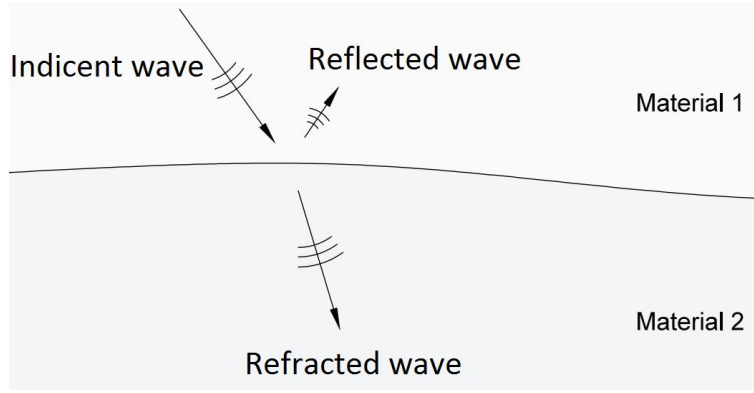
Figure 2.5: *Reflection and refraction of a wave. Figure source: [3].*

2.2.3   Material damping

In ground, when vibrations are propagating, damping will occur in the material itself. This is mainly due to micro-structural mechanisms such as friction between particles of the soil and the pore fluid viscosity. The damping can be described by a loss factor that is defined as

$$\eta = \frac{1}{2\pi}\frac{E_D}{E_S},\tag{2.4}$$

where E_D is the dissipated energy in one cycle of harmonic vibration by viscous damping and E_S is the strain energy. In a single degree of freedom system the dissipated energy may be defined as

$$E_D = \pi c \omega u^2,\tag{2.5}$$

where c is the viscous damping constant, ω is the angular frequency and u is the displacement. Furthermore, the strain energy for the same system is defined as

$$E_S = \frac{ku^2}{2},\tag{2.6}$$

where k is the stiffness of the system. Insertion of Equation 2.5 and Equation 2.6 in Equation 2.4 gives the loss factor as

$$\eta = \frac{1}{2\pi}\frac{\pi c \omega u^2}{ku^2/2} = \frac{c\omega}{k}.\tag{2.7}$$

2.3   Vibration prediction

To predict traffic-induced building vibrations the source, medium and receiver must be quantified and predicted. The increase in computational power in recent years have made it more feasible to use numerical models for these predictions.

The first step to establish a numerical model, as shown in Figure 2.6, is to identify the physical phenomena of interest and describe it with a mathematical model. In structural mechanics, such mathematical models are often constructed by differential equations based on Newton's laws of motion. An approximate solution is then sought by employing numerical methods that discretise the mathematical model, resulting in a numerical model. If the accuracy of the prediction is required to be high, calibrations and correlations to experimental results are often needed. Although, comparative studies where the investigation of different actions relative effect are studied the required accuracy is different and experimental measurements are not necessary. In the Master's thesis, no calibrations have been made between the numerical models and experimental results.

The finite element (FE) method, described further in Chapter 3, is a numerical method that can be used to study structures exposed to vibrations. Large models are expected when the FE method is used to predict traffic-induced vibrations. These models require long computational time for analysis and it can be necessary to reduce the models by using one of many reduction methods available in the literature.

In the Master's thesis, the FE method was used to model and perform analyses of both the medium and the receiver, i.e. the ground and a building. The source was considered as a harmonic load in the frequency range 5–50 Hz, which allows the harmonic response of the building to be studied.
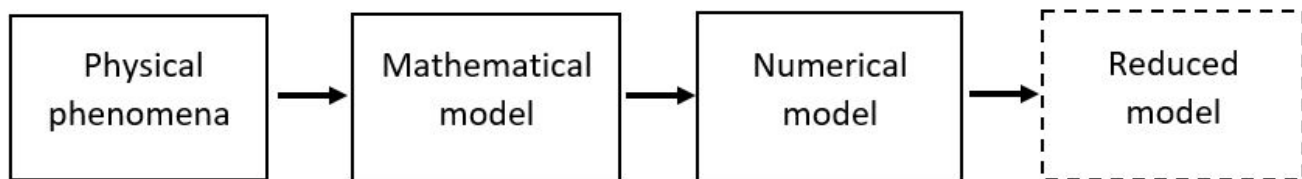
Figure 2.6: *The procedure of establishing a numerical model.*

3 Governing theory

In this chapter, an overview of the theory used for the numerical models applied in the thesis is presented.

3.1 Finite element method

The finite element (FE) method is a numerical method to solve partial differential equations (PDEs) in an approximate manner. PDEs are encountered in many engineering fields and derived from their different balance laws. As PDEs are often not suited to be solved analytically, the FE method is a practical tool to find an approximate solution. In the FE method, a FE mesh is created by dividing the geometry into smaller parts, so-called finite elements. In the finite element, the sought field variable varies according to the chosen approximation function, the shape-function, which can vary linear, quadratic or as a higher order polynomial. Each finite element have a number of nodes that holds discrete values of the sought field variable, this is the nodal degrees of freedom (dofs). If a finer FE mesh, i.e. smaller finite elements are used, the solution usually converge towards the correct answer but a finer FE mesh also means that more dofs are introduced and obtaining the solution will be more computationally costly. It means that the practicing engineer or scientist needs to balance the accuracy in the solution against the computational cost needed. The static system to be solved in the FE method can be written as

$$\mathbf{Ku} = \mathbf{f}, \tag{3.1}$$

where $\mathbf{K}$ is the stiffness matrix, $\mathbf{u}$ is the displacement vector and contains the discrete values in the nodal degrees of freedom and $\mathbf{f}$ is the external force vector. For a more detailed derivation and description, the reader is referred to the literature, for example [11].

3.2 Non-reflective boundary

In the FE method, every finite element needs a distinct boundary. This is problematic when modelling the ground that is an infinite media, where no such boundary exists in reality. If a usual finite boundary with finite elements are introduced, undesirable reflections of the propagating waves will occur. The reflected waves will superimpose with the propagating waves that can lead to inaccurate evaluations in the area of interest. Therefore, a boundary that simulate continuing propagation of the waves out of the created FE model is preferred. According to Lysmer and Kuhlemeyer [12] such a boundary can be introduced with the help of dashpots in the dofs of the boundary. Damping by a dashpot is introduced by a force proportional to the velocity, acting in the opposite direction. The magnitude of the damping coefficient in the dashpot depends on the density of the medium and the speed of the propagating wave. Two types of dashpots are introduced with different magnitude, one type in the normal direction of the boundary (d_P) and one

in the tangential directions of the boundary (d_S). In the normal direction, the damping coefficient is proportional to the P-wave speed and in the tangential directions, the damping coefficient is proportional to the S-wave speed according to

$$d_P = \rho c_P \quad \text{and} \quad d_S = \rho c_S, \tag{3.2}$$

where d_P and d_S are the damping coefficient of the dashpots, ρ are the density of the medium and c_P and c_S are the wave speed of P-waves and S-waves, respectively. The non-reflective boundary damps out P-waves and S-waves that impinge orthogonal into the boundary. In a more general case, P-waves and S-waves may not have an orthogonal angle of incidence to the boundary and furthermore other types of waves, e.g. Rayleigh waves, may occur and impinge with the boundary. However, according to [13] the non-reflective boundary is still effective as long as the strains are small, i.e. the material behaviour is linear elastic, and most waves impinge orthogonal into the boundary. Although, in the general case described above some reflection will occur and a more correct designation of the non-reflective boundary is suggested, as quiet boundary [13].

3.3   Structural dynamics

The simplest way of introducing structural dynamics in a system is to consider a single degree of freedom (sdof) system. The sdof system consists of a mass, m, a spring, k, a damper, c, and a time-dependent force, $f(t)$, and can be seen in Figure 3.1, where the Newton's second law of motion for this system gives

$$f(t) - c\dot{u} - ku = m\ddot{u}, \tag{3.3}$$

and by re-organising, it may be written as the equation of motion for a sdof system

$$m\ddot{u} + c\dot{u} + ku = f(t). \tag{3.4}$$

As structural problems usually have more than one dof, Equation 3.4 needs to be expanded to multi-degree of freedom (mdof) system. In matrix form this may be written as

$$\mathbf{M}\ddot{\mathbf{u}} + \mathbf{C}\dot{\mathbf{u}} + \mathbf{K}\mathbf{u} = \mathbf{f}(t), \tag{3.5}$$
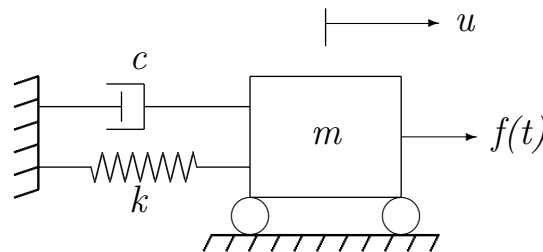
Figure 3.1: *A single degree of freedom (sdof) system with a mass, m, spring, k, and damper, c, with the time-dependent force, f(t).*

where $\mathbf{M}$ is the mass matrix, $\mathbf{C}$ is the damping matrix, $\mathbf{K}$ is the stiffness matrix and $\mathbf{u}$, $\dot{\mathbf{u}}$ and $\ddot{\mathbf{u}}$ are the displacement, velocity and acceleration vectors, respectively. The load vector, $\mathbf{f}(t)$, is time-dependent. For a more detailed description the reader is referred to literature, for example [14].

3.3.1   Resonance

Considering an undamped sdof system subjected to a harmonic force, the equation of motion can be written as

$$m\ddot{u} + ku = p_0 \sin \omega t, \tag{3.6}$$

where p_0 is the magnitude and ω is the angular frequency of the harmonic force. Equation 3.6 is a second order inhomogeneous differential equation where the solution is given by the sum of the homogeneous and particular solutions. However, as the response of the system after some time is of interest and the homogeneous solution decays over time, the particular solution is the solution of interest. A particular solution can be chosen as

$$u_p = u_0 \sin \omega t, \tag{3.7}$$

which inserted into Equation 3.6 and re-organising gives

$$u_0 = \frac{p_0}{k - m\omega^2}, \tag{3.8}$$

and it holds as long as $(k - m\omega^2) \neq 0$. Using the static response of the system

$$u_{st} = \frac{p_0}{k}, \tag{3.9}$$

one may define a non-dimensionless deformation factor as

$$\frac{u_0}{u_{st}} = \frac{p_0/(k - m\omega^2)}{p_0/k} = \frac{1}{1 - (\omega/\omega_n)^2}, \tag{3.10}$$

where $\omega_n = \sqrt{k/m}$ is denoted the eigenfrequency of the considered sdof system and Equation 3.10 holds as long as $(1 - (\omega/\omega_n)^2) \neq 0$. In Figure 3.2, it is seen that if the frequency of the harmonic load, ω, is equal to the natural frequency of the system, ω_n, the response amplitude, u, is infinite. When this phenomenon occur, the system is in resonance. In reality, damping is present in all systems, therefore the response amplitude cannot be infinite.
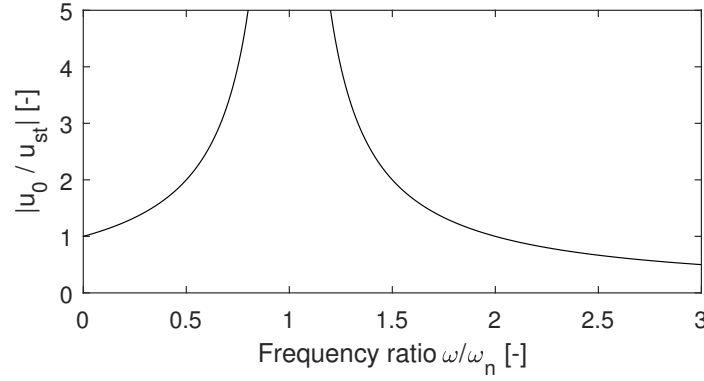
Figure 3.2: *Deformation factor for an undamped system subjected to a harmonic force with the excitation frequency ω.*

Now, considering an undamped mdof system not subjected to any load. The equation of motion for this system can be written as

$$\mathbf{M\ddot{u}} + \mathbf{Ku} = 0. \tag{3.11}$$

The solution has to satisfy the conditions at $t = 0$, i.e. the prescribed displacements and velocities. The harmonic solution

$$\mathbf{u}(t) = \hat{u}e^{i\omega t}\mathbf{\Phi}, \tag{3.12}$$

can be assumed to solve the equation of motion, where $\hat{u}$ is the complex amplitude, i the imaginary unit, ω is the angular frequency and $\mathbf{\Phi}$ is a constant vector. Differentiation of Equation 3.12 and insertion in the equation of motion, Equation 3.11, result in

$$(\mathbf{K} - \omega^2\mathbf{M})\mathbf{\Phi} = \mathbf{0}. \tag{3.13}$$

This is an eigenvalue problem with the trivial solution given by

$$\det(\mathbf{K} - \omega^2\mathbf{M}) = 0. \tag{3.14}$$

If a mdof system with m dofs is considered, there is m number of eigenfrequencies, ω_n, that solves Equation 3.14, i.e. $\omega_{n,j} = \omega_{n,1}, \ldots, \omega_{n,m}$. For each of the solutions, $\omega_{n,j}$, to Equation 3.14 there is a corresponding eigenmode, $\mathbf{\Phi}_j$, which can be determined by Equation 3.13. As an example, the first four eigenmodes of a 2D cantilever beam is illustrated in Figure 3.3. Most kinetic energy is found in the first eigenmodes [15].

(a) *Mode 1.*   (b) *Mode 2.*   (c) *Mode 3.*   (d) *Mode 4.*
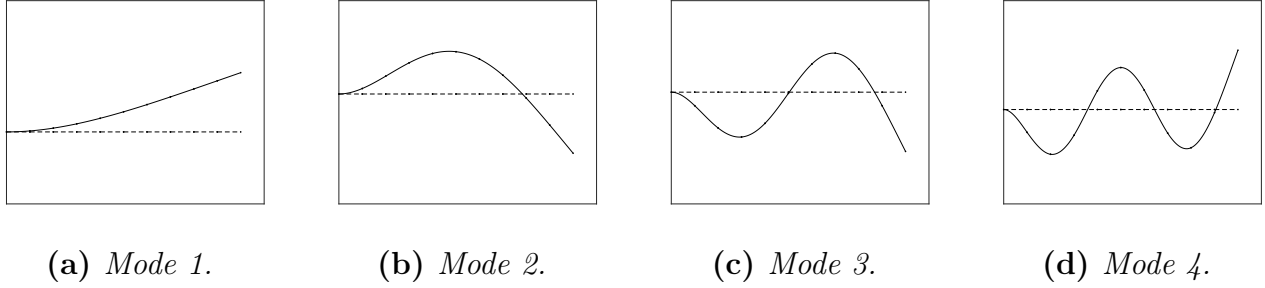
Figure 3.3: *First four eigenmodes of a 2D cantilever beam.*

3.3.2 Damping matrices

The damping of the ground and the building, described in Chapter 5 and Chapter 6 respectively, are given as a loss factor. The loss factor introduces rate-independent damping, i.e. the energy dissipation of one cycle is the same regardless of the chosen forcing frequency. Materials have different energy dissipation rates and therefore different loss factors. The rate-independent damping is introduced in the FE formulation as a stiffness proportional structural damping matrix, $\mathbf{C}_S$.

The quiet boundary described in Section 3.2 is implemented in Abaqus [13] using the dynamic formulation of the so-called infinite elements. This contributed to the viscous damping matrix, $\mathbf{C}_V$. The total damping matrix $\mathbf{C}_T$ can then be determined as

$$\mathbf{C}_T = \frac{1}{\omega}\mathbf{C}_S + \mathbf{C}_V. \tag{3.15}$$

3.3.3 Steady-state dynamics

The dynamic steady-state response in a system takes place some time after a harmonic load has been applied, i.e. the transient response has been damped out [14]. A harmonic load and the followed steady-state response can be formulated as

$$\mathbf{f}(t) = \hat{\mathbf{f}}e^{i\omega t} \quad \text{and} \quad \mathbf{u}(t) = \hat{\mathbf{u}}e^{i\omega t}, \tag{3.16}$$

where $\hat{\mathbf{f}}$ and $\hat{\mathbf{u}}$ are the complex amplitude of the load and the displacement, respectively. Insertion of the expressions in Equation 3.16 into Equation 3.5 leads to the steady-state system to solve as

$$(-\omega^2\mathbf{M} + i\omega\mathbf{C}_T + \mathbf{K})\hat{\mathbf{u}} = \hat{\mathbf{f}}, \tag{3.17}$$

where $\mathbf{C}_T$ is defined in Equation 3.15. Now a dynamic stiffness matrix, $\mathbf{D}(\omega)$, which is depended on the angular frequency is defined as

$$\mathbf{D}(\omega) = -\omega^2\mathbf{M} + i\omega\mathbf{C}_T + \mathbf{K}. \tag{3.18}$$

The steady state system in Equation 3.17 can, with the stiffness matrix in Equation 3.18, be written as

$$\mathbf{D}(\omega)\hat{\mathbf{u}} = \hat{\mathbf{f}}. \tag{3.19}$$

Steady-state analysis is a frequency-domain method, where the analysis is made with respect to frequency rather than time. However, steady-state analysis can be used to predict the time domain response of linear systems through Fourier transformation [16].

3.4   Evaluation of vibrations

Vibration levels

In order to do an evaluation of the vibration level in a steady-state analysis, it is convenient to have a comparable value. Here, the root mean square (RMS) is useful, and two definitions will be introduced, Equation 3.20 and Equation 3.21. The RMS value in Equation 3.20 is used to illustrate the variation of the vibration response between frequencies in graphs, defined as

$$V_{RMS}^I(f) = \sqrt{\frac{1}{N}\left(\sum_{i=1}^{N} V_i^2\right)}, \tag{3.20}$$

where f is the evaluated frequency, N is the number of evaluation nodes and V_i is the vertical complex velocity amplitude at the node i. The RMS value in Equation 3.21 is used to produce tabular values of the complex velocity magnitude considering all the studied frequencies, and is defined as

$$V_{RMS}^{II} = \sqrt{\frac{1}{M}\left(\sum_{j=1}^{M} V_{RMS}^I(f_j)^2\right)}, \tag{3.21}$$

where M is the number of frequency steps and $V_{RMS}^I(f_j)$ is defined in Equation 3.20. The same procedure can be used to evaluate the horizontal complex velocity magnitude (H_i), although the horizontal velocity magnitude is determined by the two horizontal complex velocity components as

$$H_i = \sqrt{H_{i,x}^2 + H_{i,y}^2}. \tag{3.22}$$

Level of inaccuracy

In a convergence study of an FE model, it is of importance to validate the accuracy of the FE model. A reference model (*ref*) can be used to calculate the *error*, in percent, of the complex velocity magnitude (V) as

$$error(f) = 100 \cdot \text{abs}\left(\frac{V - V^{ref}}{V^{ref}}\right). \tag{3.23}$$

where f is the evaluated frequency, V is the complex velocity magnitude in the model to be validated and V^{ref} is the complex velocity magnitude in the reference model. To achieve a tabular value which consider the $error(f)$ in all the studied frequencies, Equation 3.21 is used where $V_{RMS}^I(f_j)$ is replaced by $error(f_j)$ as

$$V_{RMS}^{III} = \sqrt{\frac{1}{L}\left(\sum_{j=1}^{L} error(f_j)^2\right)}, \tag{3.24}$$

where L is the number of frequency steps and $error(f_j)$ is the inaccuracy at frequency step j.

4 Developed Methodology

When the FE method is used to analyse vibrations propagating in ground, i.e the medium, large models are expected. In Chapter 5, the FE model of the ground is established and described. The computational time and memory needed to perform analyses proved to be, as expected, vast. To perform multiple analyses on a number of different buildings a reduction of the FE model was needed. In the present chapter the developed methodology, including the reduction process, is described and evaluated.

4.1   General methodology

An overview of the developed procedure is shown in Figure 4.1 as a flowchart. The final model consists of two coupled FE models, one of the ground and one of a building. The ground model is reduced after which the reduced ground model and the building model are assembled resulting in the final model. The final model is then used to conduct steady-state analyses. This allows changes to be made in the building model and new analyses to be performed without the need to implement the non-reduced ground model. Hence, the analyses become less computationally costly. The developed methodology uses two software packages, Abaqus [13] and Matlab [17].
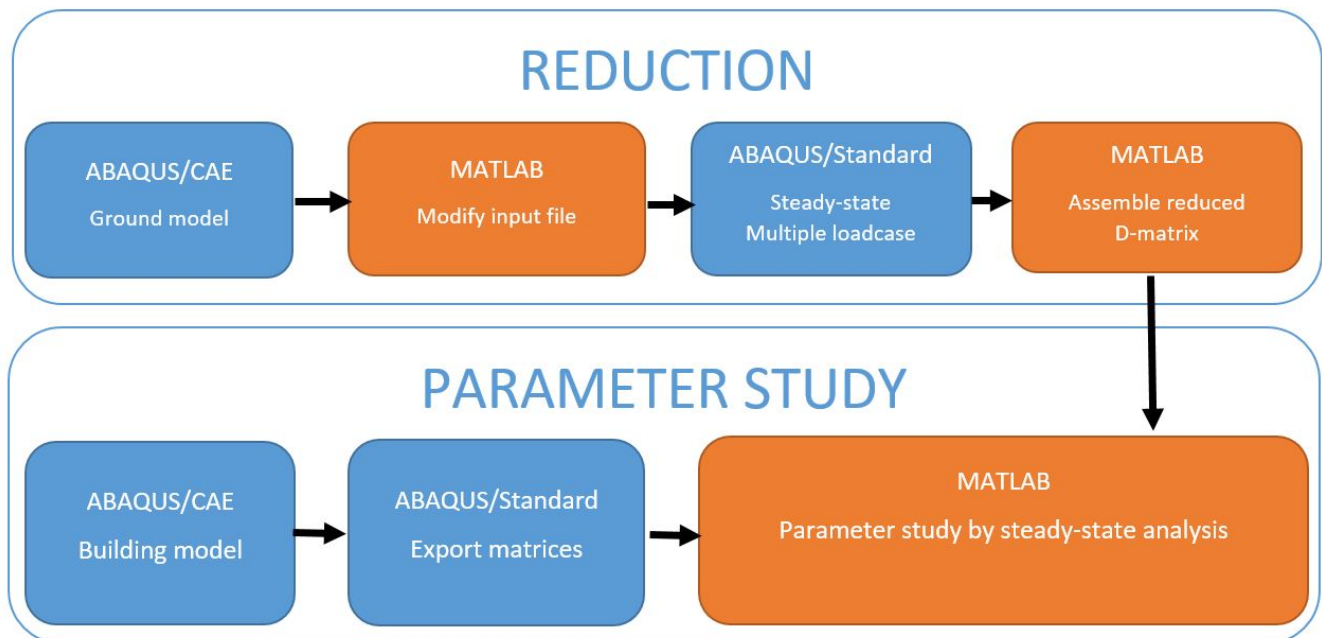
Figure 4.1: *Flowchart of analysis procedure. The two software packages used is shown in different colour, Abaqus in blue and Matlab in orange.*

The developed methodology involves two main steps:

1. **Reduction**. An FE model of the ground is created in Abaqus/CAE. The ground model is reduced by a modified version of dynamic condensation that uses Abaqus/Standard. The reduction process is described further in Section 4.2.

2. **Parameter study**. An FE model of the building is created in Abaqus/CAE. The reduced ground model and the building model is assembled and steady-state analyses are performed in Matlab. The methodology for the parameter study is described further in Section 4.3.

It is desirable to perform all numerical simulations using one specific software package in order to avoid issues when information is exchanged between two or more packages. Still, in the developed methodology two software packages are used. Including Abaqus in the methodology allows for the use of the vast amount of FE application supported in the software. However, Abaqus does not support the implement of user-defined element matrices that contain imaginary numbers. The reduced ground model can be viewed as a single finite element, a so-called *superelement*, with a dynamic stiffness matrix that contains imaginary numbers. Therefore is Matlab used to create a final model consisting of the reduced ground model and the building model.

4.2 Model reduction

In this section, the developed procedure to reduce the ground model is described beginning with a description of dynamic condensation.

4.2.1 Dynamic condensation

For steady-state analyses, fully accurate reduced models can be obtained by using dynamic condensation. When dynamic condensation is used, the dofs are divided into retained (r) and eliminated (e) that allows the steady-state system in Equation 3.19 to be partitioned as

$$\begin{bmatrix} \mathbf{D}_{rr}(\omega) & \mathbf{D}_{re}(\omega) \\ \mathbf{D}_{er}(\omega) & \mathbf{D}_{ee}(\omega) \end{bmatrix} \begin{bmatrix} \hat{\mathbf{u}}_r \\ \hat{\mathbf{u}}_e \end{bmatrix} = \begin{bmatrix} \hat{\mathbf{f}}_r \\ \hat{\mathbf{f}}_e \end{bmatrix}, \tag{4.1}$$

If it is assumed that no loads are acting on the eliminated dofs, i.e. $\hat{\mathbf{f}}_e = \mathbf{0}$, the second row in Equation 4.1 could be expanded and rewritten as

$$\hat{\mathbf{u}}_e = -\mathbf{D}_{ee}(\omega)^{-1}\mathbf{D}_{er}(\omega)\hat{\mathbf{u}}_r. \tag{4.2}$$

Expanding the first row in Equation 4.1 and insertion of Equation 4.2 results in

$$\left(\mathbf{D}_{rr}(\omega) - \mathbf{D}_{re}(\omega)\mathbf{D}_{ee}(\omega)^{-1}\mathbf{D}_{er}(\omega) \right) \hat{\mathbf{u}}_r = \hat{\mathbf{f}}_r. \tag{4.3}$$

A reduced dynamic stiffness matrix, $\tilde{\mathbf{D}}(\omega)$, can be defined as

$$\tilde{\mathbf{D}}(\omega) = \mathbf{D}_{rr}(\omega) - \mathbf{D}_{re}(\omega)\mathbf{D}_{ee}(\omega)^{-1}\mathbf{D}_{er}(\omega), \tag{4.4}$$

thus Equation 4.3 can be written as

$$\tilde{\mathbf{D}}(\omega)\hat{\mathbf{u}}_r = \hat{\mathbf{f}}_r, \tag{4.5}$$

which is the reduced steady-state system. The reduced steady-state system in Equation 4.5 provides identical results as the original system in Equation 3.19, i.e. no inaccuracy is introduced by employing dynamic condensation. In the developed methodology, the reduced dynamic stiffness matrix is sought in order to establish a final FE model of the reduced ground model and the building model. As seen in Equation 4.4, the reduced dynamic stiffness matrix can be obtained by calculating the inverse of the, usually, largest sub-block, $\mathbf{D}_{ee}(\omega)$, of the system matrix. The dynamic stiffness matrix is frequency dependant and to obtain accurate results the condensation needs to be done for each frequency of interest. The method, which is used in the developed procedure, to obtain the reduced dynamic stiffness matrix is by employing unity loading. The retained dofs are loaded with an identity matrix, $\mathbf{I}$, size $a \times a$ where a is the number of retained dofs, which allows for Equation 4.1 to be written as

$$\begin{bmatrix} \mathbf{D}_{rr}(\omega) & \mathbf{D}_{re}(\omega) \\ \mathbf{D}_{er}(\omega) & \mathbf{D}_{ee}(\omega) \end{bmatrix} \begin{bmatrix} \hat{\mathbf{u}}_r \\ \hat{\mathbf{u}}_e \end{bmatrix} = \begin{bmatrix} \mathbf{I} \\ \mathbf{0} \end{bmatrix}, \tag{4.6}$$

where $\hat{\mathbf{u}}_r$ and $\hat{\mathbf{u}}_e$ are matrices with size $a \times a$ and $b \times a$, respectively, where b is the number of eliminated dofs. $\mathbf{0}$ is a null matrix with the dimension $b \times a$. $\mathbf{D}_{rr}(\omega)$, $\mathbf{D}_{re}(\omega)$, $\mathbf{D}_{er}(\omega)$ and $\mathbf{D}_{ee}(\omega)$ are sub-blocks of the system matrix with dimensions $a \times a$, $a \times b$, $b \times a$ and $b \times b$, respectively. Expanding the rows and introduction of the reduced dynamic stiffness matrix in the same manner as above results in

$$\tilde{\mathbf{D}}(\omega)\hat{\mathbf{u}}_r = \mathbf{I} \quad \Rightarrow \quad \hat{\mathbf{u}}_r = \tilde{\mathbf{D}}^{-1}(\omega). \tag{4.7}$$

The reduced dynamic stiffness matrix can therefore be obtained by solving the linear equation system in Equation 4.6 and then finding the inverse of the resulting $\hat{\mathbf{u}}_r$ matrix.

4.2.2 Reduction methodology
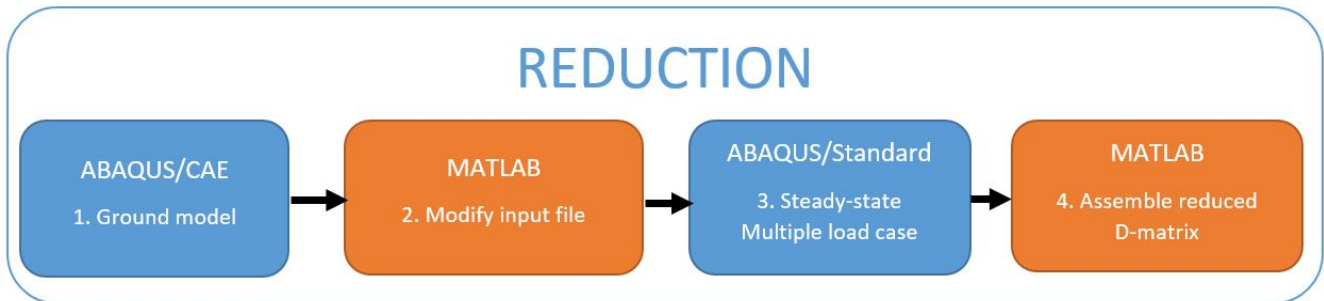
Figure 4.2: *Flowchart of developed reduction procedure. The two software packages used is shown in different colour, Abaqus in blue and Matlab in orange.*

The developed reduction methodology, illustrated in Figure 4.2 as a flowchart, involves the following steps:

1. **Creation of FE model.** An FE model of the ground is created using Abaqus/CAE. A direct-solution steady-state dynamic analysis step is added.

2. **Load cases.** The load cases are added by modifying the input file using a Matlab script. In each load case, a retained dof is loaded with 1 N. The amount of load cases are the same as the number of retained dofs.

3. **Solve**. A steady-state multiple load case analysis is performed in Abaqus/Standard to obtain the solution to the linear system in Equation 4.6. The results for the retained dofs are saved.

4. **Reduced matrix.** A python script is used to extract the results from Abaqus and to write the results to a text file. These results are imported to Matlab where the reduced dynamic compliance matrix, $\tilde{\mathbf{D}}^{-1}(\omega)$, is assembled and inversed to obtain the reduced dynamic stiffness matrix, $\tilde{\mathbf{D}}(\omega)$. In this manner, a reduced matrix is produced for each frequency of interest.

The developed reduction methodology makes use of Abaqus capability to perform multiple load case analysis. This type of analysis allows for a set of loads in the same step, which is generally more effective than the equivalent multiple step analysis where each step contains just one load condition. However, multiple load case analysis may consume more memory and disk space [13].

In the Master's thesis, the FE ground model described in Chapter 5 was reduced by the developed methodology. The steady-state analysis was performed over the frequency range 5–50 Hz with 1 Hz steps and using 1446 load cases. The analysis was conducted using the Lunarc computer cluster *Aurora* [18] with 20 CPU's in parallel and 62 GB available working memory. The suggested memory from Abaqus to minimize computational time was approximately 300 GB but only 5 GB was required to perform the analysis. For each individual frequency, the reduction process took around 5 hours to complete and produced full complex matrices with the size 1446×1446 that could be managed by a common desktop computer.

4.2.3   Area of interest

Before the reduction of an FE model can be performed, the area of interest needs to be established. When analysing traffic-induced building vibrations, the area of interest may be the surface of the ground where the investigated building is located or going to be built. It could be a new construction site or an existing building that will be investigated. The dofs contained in the area of interest will be the retained dofs of the FE model, i.e. the remaining dofs in the reduced FE model. For the parameter study performed in the thesis, the area of interest consisted of a square shaped area (15×15 m^2) of the ground surface and a node placed 20 m from the square area. This choice enables analyses on buildings with footprints of up to 225 m^2 when the building is subjected to a load 20 m away. The area of interest in the FE ground model can be seen in Figure 4.3, where it is coloured in red.
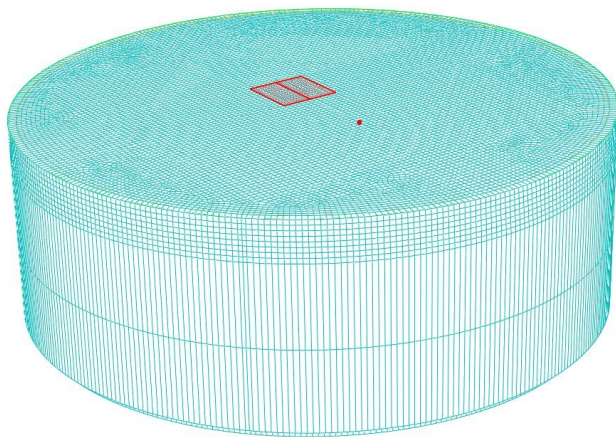
Figure 4.3: *Graphic representation of the reduced FE ground model where the area of interest, i.e. the retained dofs, are coloured in red.*

4.3   Parameter study

As mentioned in Section 4.1, Matlab is used to perform the parameter study with steady-state analyses. Matlab is used instead of Abaqus because of Abaqus lack of implementation capabilities for user defined element matrices that contain imaginary numbers. However, Abaqus is still used to create the building models. The developed parameter study methodology, illustrated in Figure 4.4 as a flowchart, involves the following steps:

1. **Creation of FE model**. An FE model of the investigated building is created using Abaqus/CAE.

2. **Export matrices**. The mass, stiffness and damping matrix of the building model are exported with Abaqus/Standard.

3. **Topology and assembly**. The exported matrices are converted to Matlab sparse format and a dynamic stiffness matrix of the building model is calculated as in Equation 3.18. Global topology of the final model, consisting of both the reduced ground model and the building model, is establish and a global dynamic stiffness matrix, $\mathbf{D}_{global}(\omega)$, is created accordingly. Thus a frequency dependent steady-state system is established,

$$\mathbf{D}_{global}(\omega)\hat{\mathbf{u}} = \hat{\mathbf{f}}. \tag{4.8}$$

4. **Solve.** The unknown complex displacement amplitudes, $\hat{\mathbf{u}}$, are computed by solving the linear system in Equation 4.8 using the Matlab function mldivide. Velocities and RMS values are evaluated.

5. **Visualisation**. The response of the building can be visualised in animated harmonic 3D scatter plots.
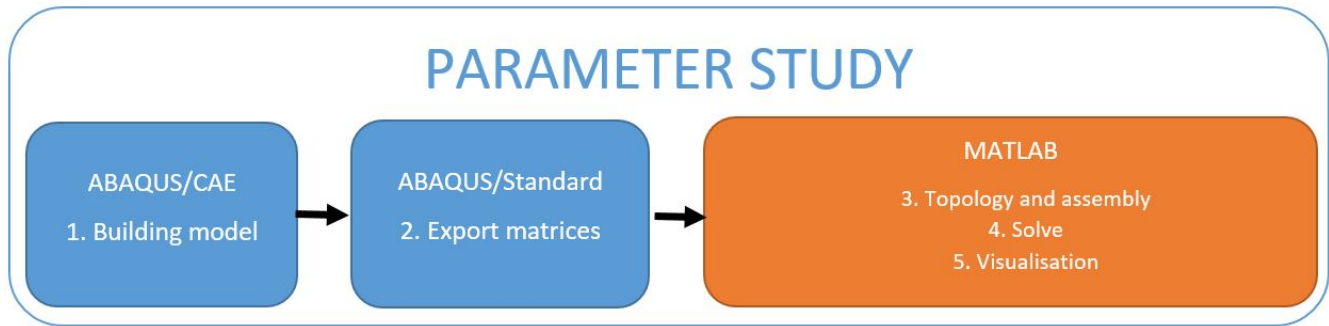
Figure 4.4: *Flowchart of developed parameter study procedure. The two software packages used are shown in different colour, Abaqus in blue and Matlab in orange.*

The coupling of the building model to the reduced ground model is performed by coupling coinciding nodes and no constraints are used at their interface. Therefore, the two meshes could only be connected by using nodes common to each mesh. This limits the meshes to be the same size at the interface between the reduced ground model and the building model. In order to keep track of the nodes and to know how the nodes are related to each other, in Abaqus and Matlab, a global cartesian coordinate system is used. The coordinates of the nodes in the area of interest are extracted from the ground model and introduced in the building model as geometric points (denoted as *datum points* in Abaqus). The building model is then placed to match these points. In that way, the coinciding dofs between the ground model and the building model are provided by a comparison of the nodal coordinates.

The ground model, described in Chapter 5, was used to test the performance of the developed parameter study methodology. Steady-state analysis at one frequency took 965 s when using the solver implemented in Abaqus/Standard 6.14 on two Intel Xeon E5-2650 v3 ten-core processors of 2.3 GHz and with 62 GB of available working memory. Using the reduced ground model and the developed parameter study methodology on the same processors resulted in a computing time of 2.8 s. Thus by performing the reduction, the computational time for the steady-state analysis in the parameter study was reduced by 99.7%. Also, maybe more convenient, the parameter study could be performed on a common desktop computer.

In Table 4.1 computational time for steady-state analyses using the developed methodology is shown. Analyses on building models with different amount of dofs were performed and clocked using a desktop computer with Intel Core i5 3.4 GHz processor and 4 GB of available working memory. The building FE models used to investigate the influence of different structural design choices, described in Chapter 6, contained approximately 30 000 dofs.

Table 4.1: *Performance of the developed parameter study methodology with implementation of a reduced ground model. Computational time for converting to sparse format and to solve using building models with varying amount of dofs are shown. Note that the conversion to sparse format is only done once while the solving is done for each frequency of interest.*

Number of dofs in building model	Convert to sparse [s]	Solving [s/frequency]
30 000	4.1	2.1
50 000	8.0	3.1
70 000	10.8	4.2
100 000	17.1	5.5
200 000	51.2	14.6

The steady-state system is solved by employing the Matlab function mldivide, also known as backslash. Mldivide is an optimised toolbox which includes a set of routines for solving sparse linear systems such as in Equation 4.8 [19]. Mldivide uses direct methods to solve the linear system that, in contrast to iterative methods, obtains the solution in a finite and fixed number of steps. For a more detailed description of the direct method, see [20]. When the system matrix is complex and sparse, as the global dynamic stiffness matrix, a direct method is used which includes LU decomposition. LU decomposition factors the matrix as the product of a lower triangular matrix and an upper triangular matrix, i.e.

$$\mathbf{D} = \mathbf{LU} \tag{4.9}$$

where $\mathbf{L}$ and $\mathbf{U}$ are the lower and upper triangular matrix, respectively. A triangular matrix is a square matrix where all the entries above or under the main diagonal are zero. LU decomposition of large matrices requires access to large amounts of computer memory. In Matlab, the minimum required memory to store a sparse, square and complex matrix with dimensions n x n and nnz non-zero elements is [21]:

$$24 \times nnz + (n+1) \times 8 \quad [\text{bytes}]. \tag{4.10}$$

The triangular matrices constructed during the LU decomposition does not always retain the same amount of non-zero elements as the matrix they factored. Tests were made on different dynamic stiffness matrices and the number of non-zero elements in the triangular matrices increased with up to ten times as many as the nnz elements in the original matrix. This indicates that more than three times the memory allocation of the dynamic stiffness matrix is needed when the direct method is used to solve a linear system such as in Equation 4.8.

4.4   Conclusion

A reduction of a large FE model by the methodology described in Section 4.2.2 is computationally costly. However, the methodology is easy to implement in Abaqus by the multiple load case option and the computational cost to perform analyses with the reduced system decreases greatly. The number of retained dofs influence the computational time to perform both the reduction and the parameter study. A larger number of retained dofs leads to more load cases in Abaqus which

requires more computational resources. In addition, the size of the reduced dynamic stiffness matrix is dependent on the number of retained dofs.

Analysis on building models with up to 200 000 dofs is possible using the developed parameter study methodology, as can be seen in Table 4.1. Although the computing time increases for larger models, the elapsed time is still considerably less than the time it took to perform analyses using the non-reduced ground model. This indicates that the direct-method used in the developed parameter study methodology is fast to use even for larger models. However, the required memory is likely to be vast if the final model gets too big. For example, the non-reduced FE ground model contained around 1.4 million dofs and had a dynamic stiffness matrix with around 4 billion non-zero elements. To store this dynamic stiffness matrix in Matlab would require a minimum of 96 GB of available memory and employing the direct-method would require at least three times the memory, which is not feasible.

The general methodology was developed to investigate the influence of structural design on traffic-induced vibrations. However, the developed methodology is also suited for other applications when a large FE model needs to be reduced.

5 Numerical ground model

The medium, in which the generated vibrations propagate, needs to be included in the numerical simulations in order to predict the vibration levels at the receiver. Here, the medium is the ground between the source and the receiver. Therefore, an FE model of the ground was established.

5.1   Material

The dynamic material parameters of the ground were chosen by studying the evaluations performed at the construction site of The Max IV Laboratory in Lund [22]. The ground model was chosen to consist of a 10 m deep soil layer, consisting of a rather stiff clay till, on top of the bedrock. The material parameters of the soil and the bedrock can be seen in Figure 5.1. The damping of the ground was given as a material parameter, the loss factor.

With the parameters in Figure 5.1 and the equations in Section 2.2.1, the velocity of P-waves, S-waves and Rayleigh waves can be determined in the soil and the bedrock, respectively. The wave velocities can be seen in Table 5.1.

Soil

$\rho = 2000 \ \text{kg/m}^3$
$E = 500 \ \text{MPa}$
$v = 0.48$
$\eta = 0.1$

10 m

Bedrock

$\rho = 2500 \ \text{kg/m}^3$
$E = 10\,000 \ \text{MPa}$
$v = 0.40$
$\eta = 0.04$
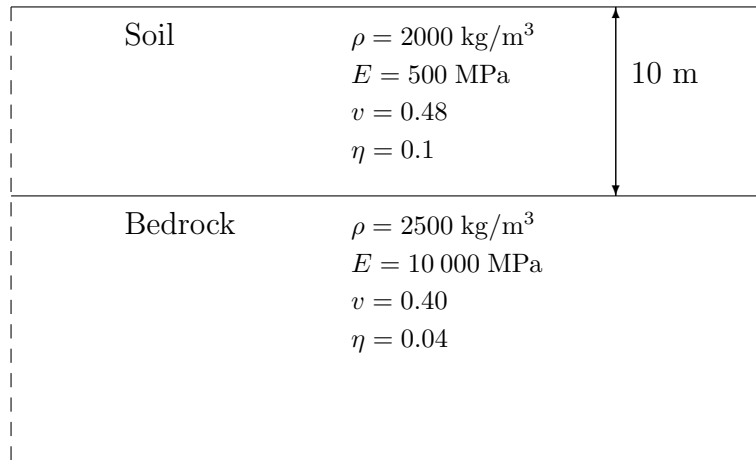
Figure 5.1: *The mass density (ρ), Young's modulus (E), Poisson's ratio (v) and loss factor (η) of the soil and the bedrock. The depth of the soil layer is 10 m.*

Table 5.1: *The velocity of pressure (c_P), shear (c_S) and Rayleigh (c_R) waves in the soil and in the bedrock.*

	c_P [m/s]	c_S [m/s]	c_R [m/s]
Soil	1482	291	262
Bedrock	2 928	1 195	1 076

5.1.1   Homogeneity

The ground is in general a heterogeneous material where the size of the particles differs throughout the medium, from small clay particles to large boulders. Although, the shortest wavelength is still significant longer compared to the largest particle size in the soil. For example the highest studied frequency, 50 Hz, gives the shortest wavelength of 5.2 m. Therefore, it is valid to model the ground as a homogeneous material.

5.1.2   Constitutive relation

General speaking the ground cannot be modelled as linear elastic, e.g. when studying earthquakes. These large strains would result in cracking and non-linear behaviour. However, when studying traffic induced vibrations the strains in the ground are in general small. Although, close to the source of traffic induced vibrations non-linear behaviour in the ground might occur. As the studied vibrations takes place some distance from the source this effect can be neglected, i.e. a linear elastic material model can be used to model the ground.

5.2   Geometric domain

In general, the ground is an infinite medium that cannot be modelled in its entirety and therefore a finite geometric domain was needed. The vibration source was applied as a point load that generated body waves and surface waves, which is illustrated in Figure 2.4. As quiet boundaries, described in Section 3.2, will be used in the model and they are more effective if most waves impinge orthogonal into the boundary a cylindrical geometry of the FE model was preferable. It was also noticed that using a cylindrical model resulted in an FE model with a smaller number of dofs compared to a rectangular cuboid model with the same length across the surface as the diameter of cylindrical model. As the computational cost of an FE analysis is less with a decreased number of dofs, a cylindrical model was preferable also for this reason.

(a) *Radius and depth of the model.*   **(b)** *Top view.*
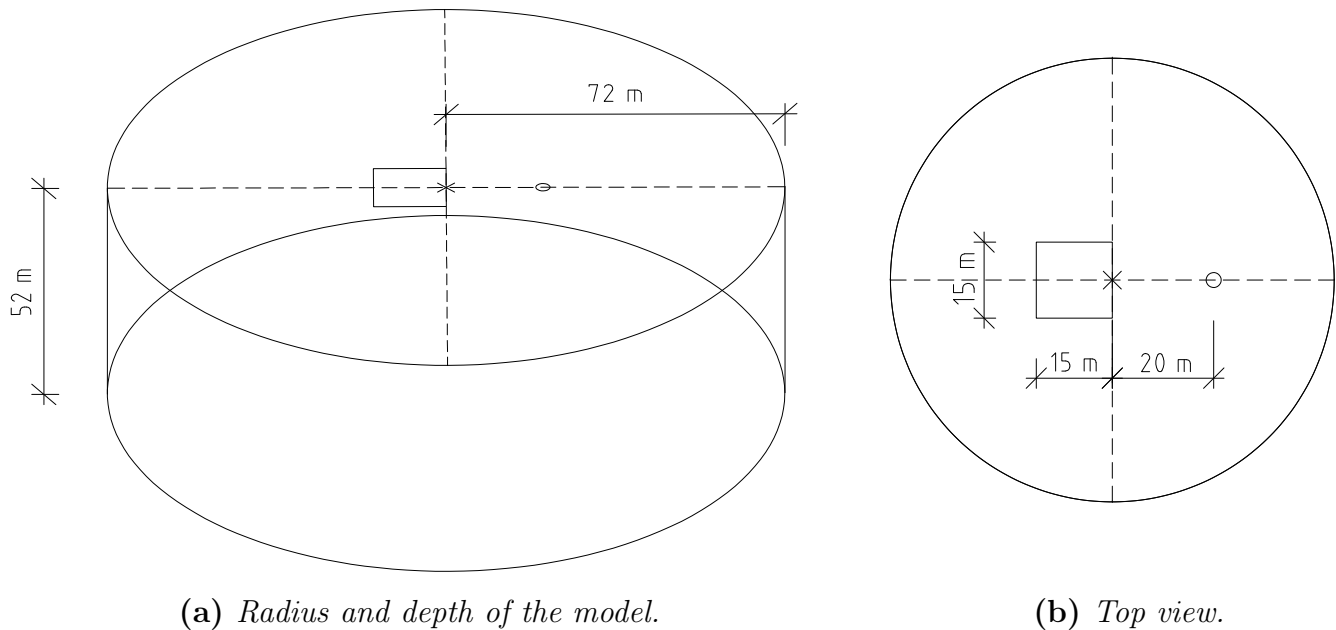
Figure 5.2: *The geometry of the cylindrical model where the centre point (×) and the area of interest, i.e. the 15×15 m^2 rectangle and load node (circle) can be seen.*

As mentioned, a cylindrical geometry was used to both minimise the dofs in the model and increase the efficiency of the quite boundaries. The convergence studies (see Subsection 5.4.5) indicated that the cylindrical model needed to be 50 m deep. The convergence studies also showed that the width must be chosen in a way that the infinite boundary is located 50 m from the load. The reduction method used includes loading of all retained dofs thus the distance between all the dofs in the area of interest and the infinite boundary must be at least 50 m. With the surface in the area of interest being 15×15 m^2, the dof of interest closest to the boundary is in the loading node, which is marked with a circle in Figure 5.2. With a distance between the loading node and the centre point set to 20 m, the radius of the cylinder had to be 70 m. The length of the infinite elements was 2 m, which produces the final cylindrical FE model that can be seen in Figure 5.2, with the depth and the width of 52 m and 72 m, respectively.

The model was created as one part with two different sections. One section containing the 10 m deep soil layer and the other section containing the bedrock. The model was partitioned as in Figure 5.3, where the area of interest, i.e. the 15×15 m^2 square and the loading node, was included into a geometry set. The geometry set would then contain all the retained dofs.

5.3   Mesh and element types

The mesh consisted of 20-node 3D quadratic brick elements with reduced integration (denoted C3D20R in Abaqus) and 12-node 3D infinite elements (denoted CIN3D12R in Abaqus). The infinite elements introduced the quiet boundaries in the FE model. These infinite elements were not supported in the Abaqus user interface, Abaqus/CAE, therefore were these regions (see green regions in Figure 5.3) meshed with a different element type from the already used, 20-node 3D quadratic brick element. Here, the linear pressure hybrid element (denoted C3D20RH in Abaqus) was

(a) *Top view.*   (b) *Cross-section view.*
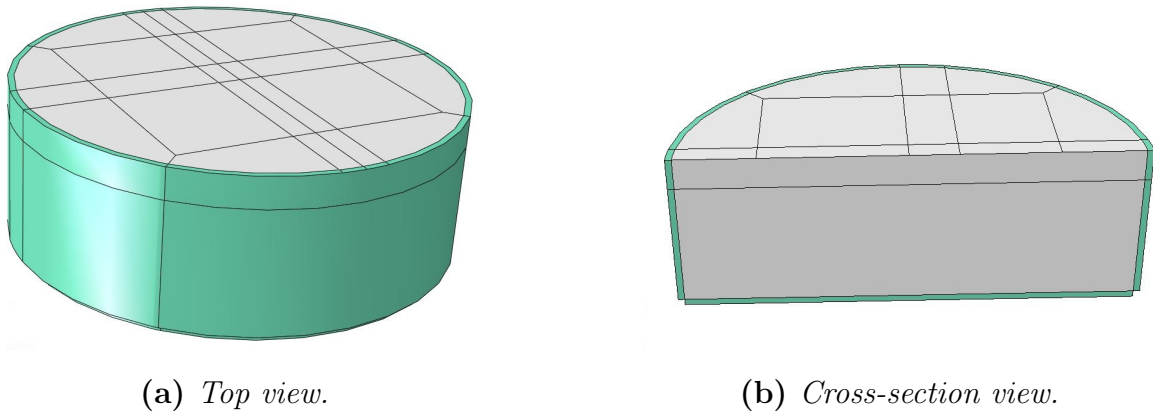
Figure 5.3: *The distribution of different element types, green regions with 12-node 3D infinite elements and the grey region consisted of 20-node 3D quadratic brick elements with reduced integration.*

chosen. By modifying the input file, the hybrid elements could be exchanged for the desired 12-node 3D infinite elements. Although, the hybrid elements had to be stacked in a way that the node numbering were known and the correct surface of the 12-node 3D infinite elements could be connected to the used 20-node 3D quadratic brick elements.

An element size of $1.25\times1.25\times1.25$ m^3 were used for the 20-node 3D quadratic brick elements, besides in the bedrock z-direction where the length was 20 m. The element sizes were chosen in accordance with the convergence studies. The element size of the 12-node 3D infinite elements was the same as the brick elements except in the outward direction of the model that was set to 2 m. This resulted in a model with 101 540 brick elements and 13 634 infinite elements, which resulted in approximately 1.4 million dofs. The mesh of the cylindrical FE ground model is shown in Figure 5.4.

(a) *Top view.*   (b) *Side view.*
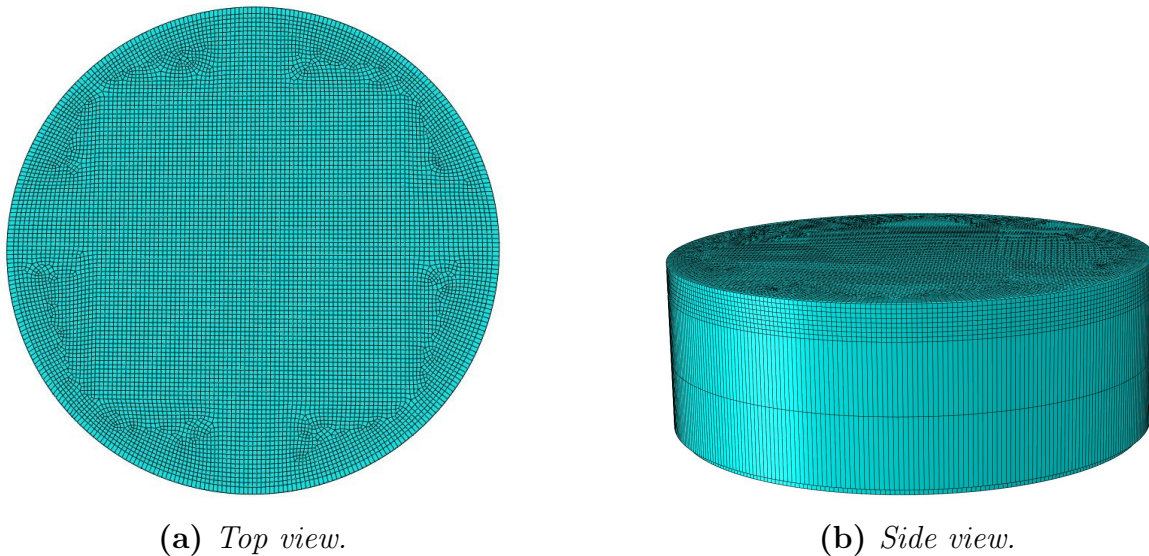
Figure 5.4: *FE mesh of the cylindrical ground model.*

5.4   Convergence studies

It is important that simulations, using the cylindrical FE model, give reliable results within the area of interest without being too computationally costly, i.e. having an FE model with to many dofs. Therefore, convergence studies have been conducted to determine the properties of the cylindrical FE model, such as the depth, radius and the element size. In each convergence study, one of the three properties was altered while the others were kept constant. To perform the convergence studies, the cylindrical model was simplified into an axisymmetric model. In the axisymmetric model, any point (except in the axial symmetry line) represents a circle, which is illustrated in Figure 5.5.

An introduced uncertainty in the FE model that can affect the result was the quiet boundary, which reflects the propagating waves in some extent. That is why the quiet boundary was placed some distance from the area of interest in order to allow the reflected waves to be damped out before reaching the area of interest. As the distance increases, the model become geometrically larger and the number of dofs in the FE model increases.

The size of the finite elements in the FE model determined the accuracy in the simulations of the propagating waves, i.e. the elements had to be small enough to produce reliable results. However, using smaller elements would increase the number of dofs in the FE model.

The result in the convergence studies was the vertical complex velocity magnitude of the vibration on the soil surface 5 m and 20 m from the load. The result 5 m from the load indicated on the least distance to the quiet boundary, for the reflected waves to be damped. The result 20 m from the load indicated both the least distance to the quiet boundary but also what element size to use, to achieve reliable results within a radius of 20 m around the load.

In Figures 5.8–5.13 the vertical complex velocity magnitude (V_y), in the performed convergence studies, can be seen. Logarithmic y-axis have been used in these figures in order to present the result in a clearer way. In Tables 5.2–5.4 the RMS value of the error can be seen when altering a property. The error has been calculated as a percentage difference to a reference model at each frequency, according to Equation 3.23, and the RMS value of the error was calculated according to Equation 3.24.
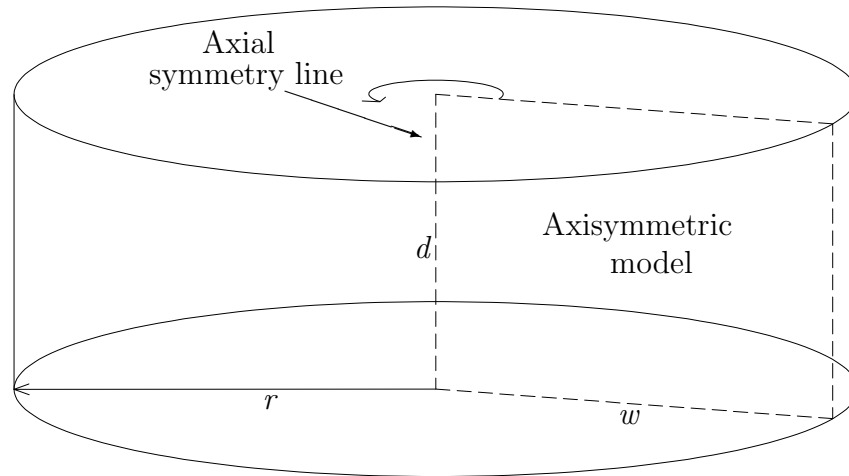
Figure 5.5: *The axisymmetric model (dashed rectangle) represents a cylindrical model. The width (w) of the axisymmetric model equals to the radius (r) of the cylindrical model where both models have the same depth (d).*

5.4.1   Axisymmetric model

In the axisymmetric model (see Figure 5.6), there is a 10 m soil layer on top of the bedrock. The material parameters of the ground can be seen in Figure 5.1. The left vertical boundary was an axial symmetry line by prescribing the horisontal displacement along the boundary and quiet boundaries were used along the bottom horisontal boundary and the right vertical boundary. In the top left corner, a vertical unit load was applied.

The mesh of the axisymmetric FE model, which can be seen in Figure 5.7b, consisted of 8-node
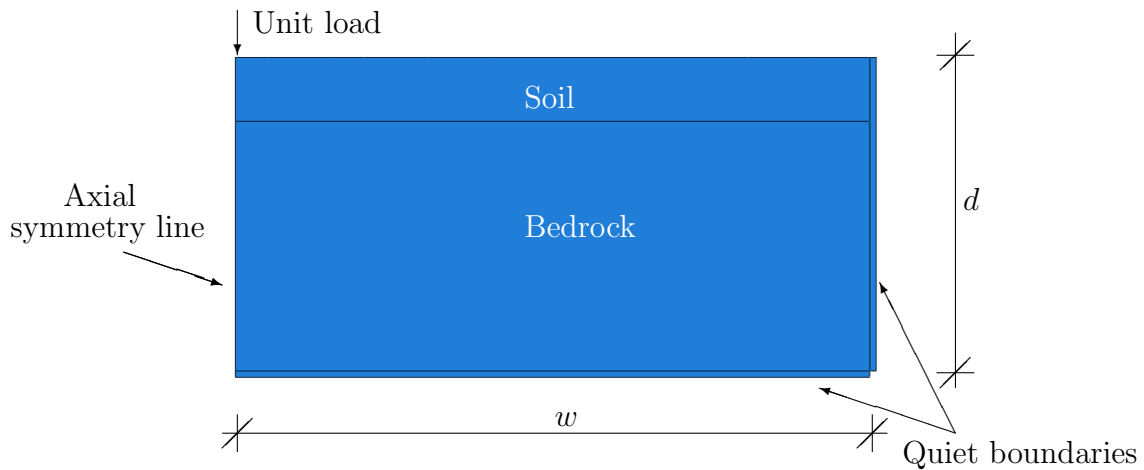
Figure 5.6: *Axisymmetric FE model with the width, w, and the depth, d. A vertical unit load is applied in the top left corner, axial symmetry is applied along the left vertical boundary and quiet boundaries are used along the bottom and the right vertical boundary.*

(a) *Green regions with the 5-node infinite elements and the grey regions with the 8-node elements.*

(b) *FE mesh of the axisymmetric model.*
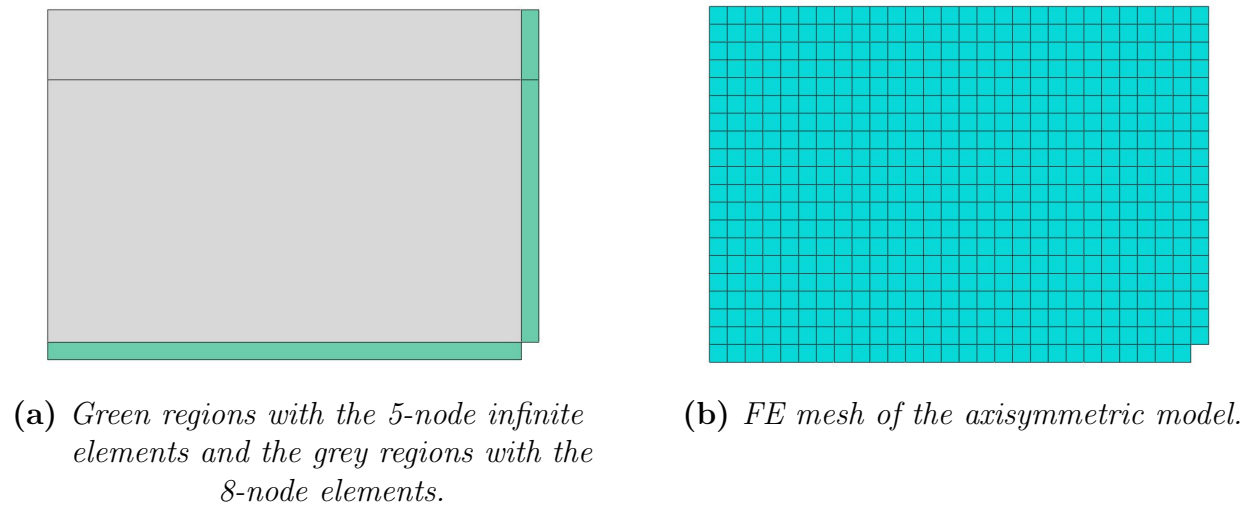
Figure 5.7: *The distribution of different element types and the FE mesh of the axisymmetric model used in the convergence studies.*

biquadratic axisymmetric elements with reduced integration (denoted CAX8R in Abaqus) in the gray regions in Figure 5.7a and the 5-node quadratic axisymmetric infinite elements (denoted as CINAX5R in Abaqus) in the green regions in Figure 5.7a. The infinite elements introduced the quiet boundaries in the model but they were not supported in the Abaqus user interface, Abaqus CAE. Although, the procedure was analogous with including the 12-node 3D infinite elements in the cylindrical model and the procedure is described in Section 5.3. The different element type that was exchanged for the infinite elements was chosen as 8-node biquadratic axisymmetric elements (denoted as CAX8 in Abaqus). A structured mesh was chosen in order to reduce the effect of the meshing style on the result.

5.4.2   Width

In the width convergence study, the depth was set to 100 m and an element size of $2.5{\times}2.5$ m^2 was used, while the width was set to 30, 50, 70, 100 and 200 m. In Figure 5.8 and Figure 5.9 is the vertical complex velocity magnitude at the soil surface presented, obtained 5 m and 20 m from the load. In Table 5.2, the RMS value of the error can be seen, evaluated 5 m and 20 m from the load.
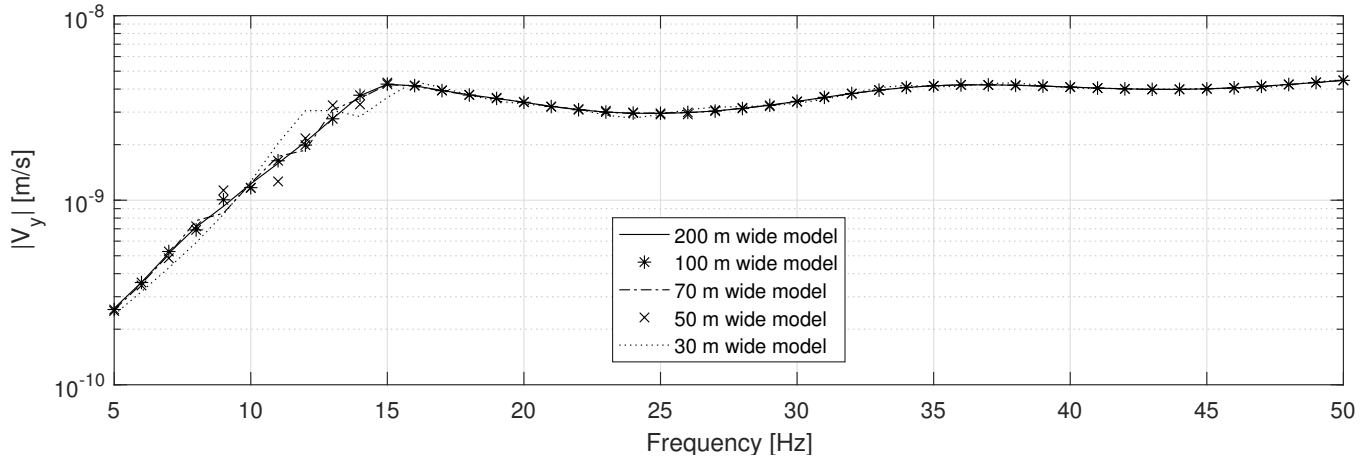
Figure 5.8: *Vertical complex velocity magnitude at the soil surface, obtained 5 m from the load, for models with different width.*
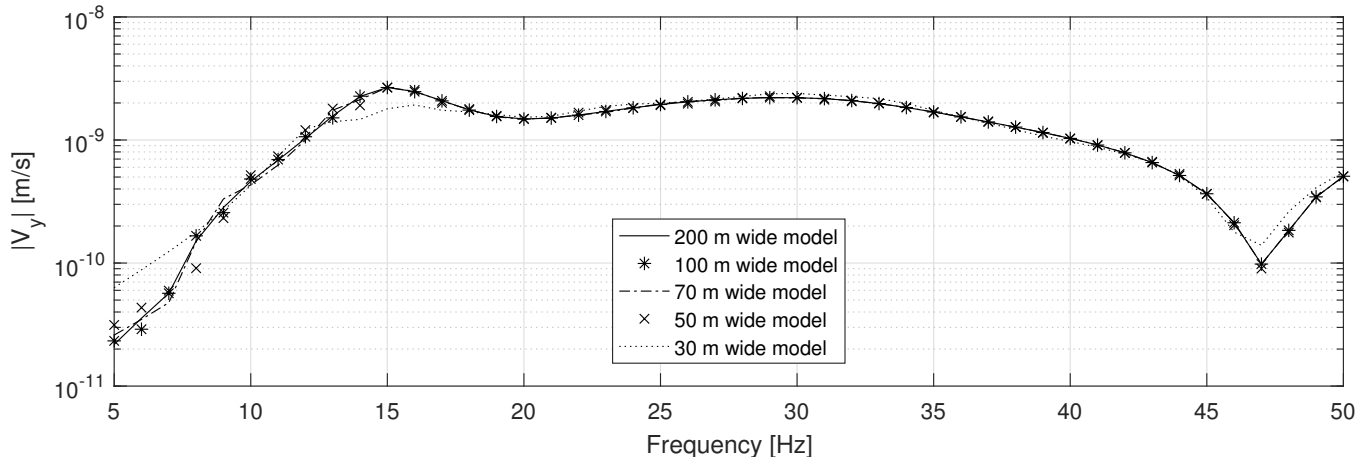
Figure 5.9: *Vertical complex velocity magnitude at the soil surface, obtained 20 m from the load, for models with different width.*

Table 5.2: *The error of the vertical complex velocity magnitude at the soil surface presented as a RMS value for models with different width, evaluated 5 m and 20 m from the load. The reference model had a width of 200 m.*

Model width [m]	RMS value of the error [%]	
	5 m from load	20 m from load
100	1.73	3.69
70	3.23	5.21
50	5.63	10.95
30	10.46	41.86

5.4.3 Depth

In the depth convergence study, the width was set to 100 m and an element size of 2.5×2.5 m^2 was used, while the depth was set to 30, 50, 70 and 100 m. In Figure 5.10 and Figure 5.11 is the vertical complex velocity magnitude at the soil surface presented, obtained 5 m and 20 m from the load. In Table 5.3, the RMS value of the error can be seen, evaluated 5 m and 20 m from the load.
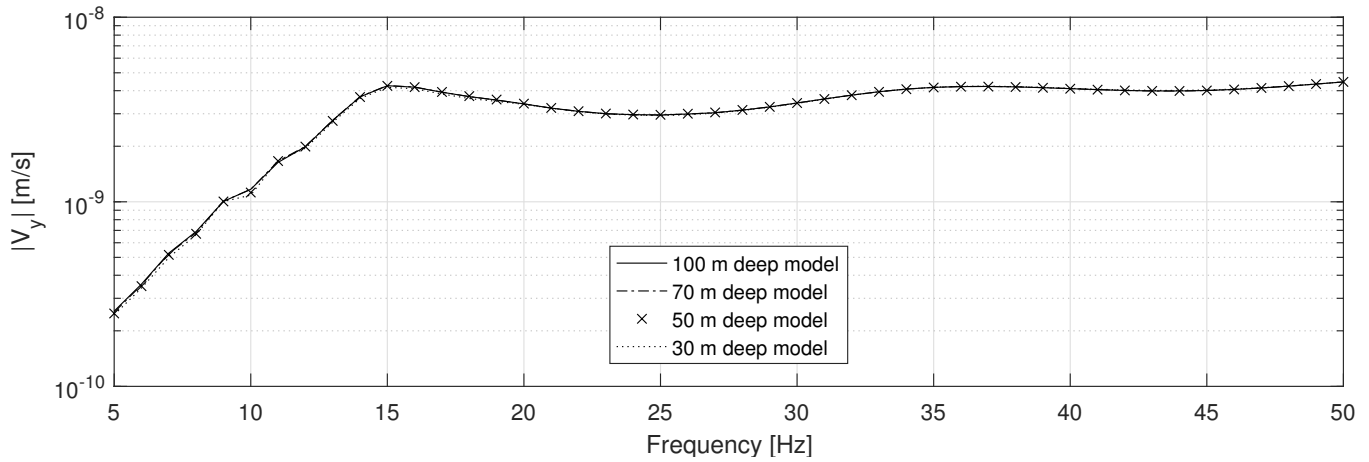
Figure 5.10: *Vertical complex velocity magnitude at the soil surface, obtained 5 m from the load, for models with different depth.*
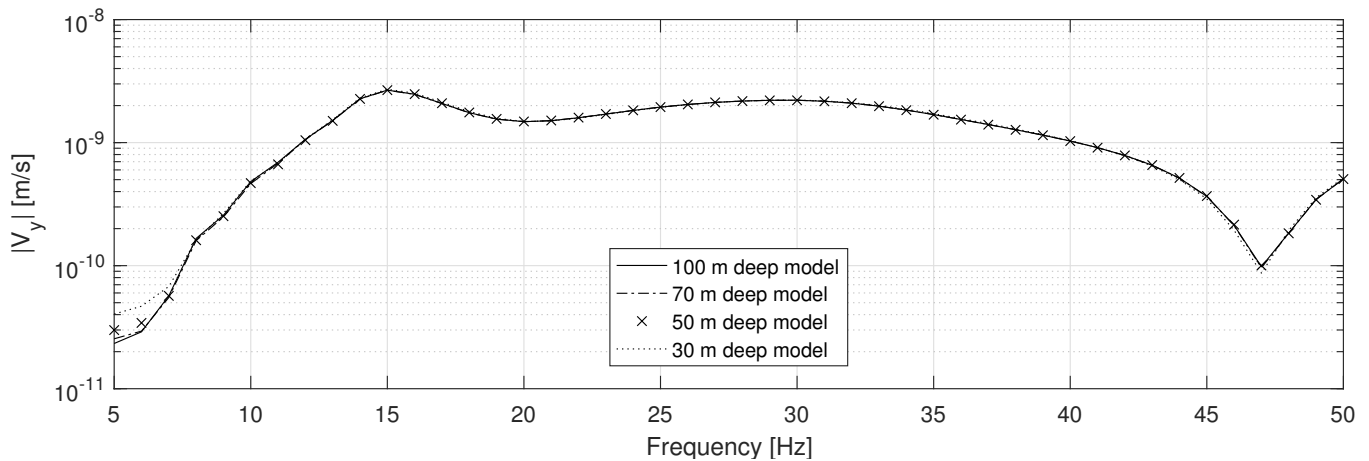
Figure 5.11: *Vertical complex velocity magnitude at the soil surface, obtained 20 m from the load, for models with different depth.*

Table 5.3: *The error of the vertical complex velocity magnitude at the soil surface presented as a RMS value for models with different depth, evaluated 5 m and 20 m from the load. The reference model had a depth of 100 m.*

Model depth [m]	RMS value of the error [%]	
	5 m from load	20 m from load
70	0.42	1.76
50	1.02	5.09
30	1.99	14.68

5.4.4   Finite element size

In the finite element size convergence studies, the depth and the width were set to 50 m and 70 m, respectively. Here, two studies were conducted, an element size study of the entire FE model and a study of the element size in the bedrock.

In the element size study of the entire FE model, the element size was altered in both the soil and the bedrock between 0.5×0.5, 0.83×0.83, 1.25×1.25, 1.67×1.67 and 2.5×2.5 m². In the study of the element size in the bedrock, the element size in the soil was set to 1.25×1.25 m² and the element size in the bedrock was altered between 1.25×1.25, 1.25×10 and 1.25×20 m².

In Figure 5.12 and Figure 5.13, the vertical complex velocity magnitude at the soil surface 20 m from the load is presented for the two studies, respectively. In Table 5.4 the RMS value of the error can be seen, evaluated 20 m from the load.
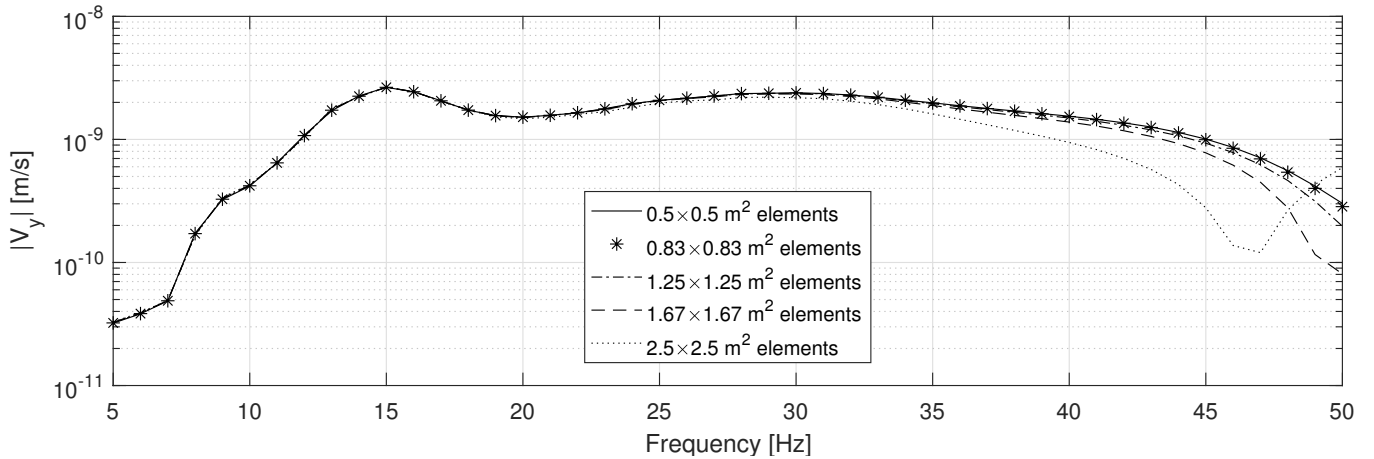
Figure 5.12: *Vertical complex velocity magnitude at the soil surface, obtained 20 m from the load, for models with different element size in the entire FE model.*
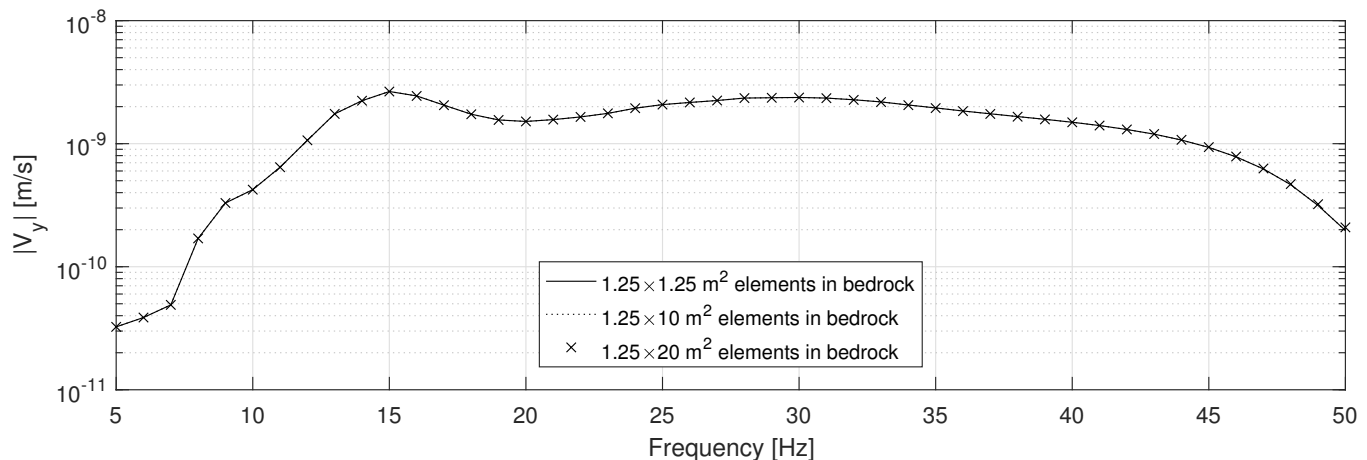
Figure 5.13: *Vertical complex velocity magnitude at the soil surface, obtained 20 m from the load, for models with different element size in the bedrock.*

Table 5.4: *The error of the vertical complex velocity magnitude at the soil surface presented as a RMS value for models with different element size, evaluated 20 m from the load.*

(a) *The reference model had an element size of 0.5×0.5 m^2.*

Element size in all the model [m^2]	RMS value of the error [%]
0.83×0.83	1.28
1×1	2.92
1.25×1.25	7.43
1.67×1.67	19.30
2.5×2.5	32.44

(b) *The reference model had an element size of 1.25 × 1.25 m^2 in the bedrock.*

Element size in the bedrock [m^2]	RMS value of the error [%]
1.25×10	0.01
1.25×20	0.99

5.4.5   Conclusions

In the width convergence study, a width of 50 m, had a 5.63% RMS value of the error evaluated 5 m from the load and a width of 70 m, had a 5.21% RMS value of the error evaluated 20 m from the load, which is seen in Table 5.2. In the depth convergence study, a depth of 50 m had 1.02% and 5.21% RMS values of the error evaluated 5 m and 20 m from the load, respectively, which is seen in Table 5.3. In the element size convergence studies, the element size of 1.25×1.25 m^2 in the entire model, had a 7.43% RMS value of the error, which is seen in Table 5.4a and by altering the element size in the bedrock to 1.25×20 m^2, a 0.99% RMS value of the error was given, which is seen in Table 5.4b.

The summarised results in the above conclude that the quiet boundary in the FE model needs to be located at least 50 m from the closest node of interest and a depth of 50 m is needed. The element size in the FE model are chosen to be 1.25×1.25 m^2 in the soil and 1.25×20 m^2 in the bedrock, to produce reliable results.

6 Structural modifications

The receiver, which the traffic-induced vibrations affect, is often a building. To predict and compare obtained vibration levels inside the building, the building itself needs to be included in the numerical simulations. In the present chapter, FE models of two reference buildings are constructed, a heavy-weight building in concrete and a light-weight building in wood. Different design choices are then evaluated in a parameter study.

6.1   Reference building

The geometry of the reference building is shown in Figure 6.1. The building consists of two frames with slabs spanning between. The top slab is the roof and the other two slabs are the first and second floor of the building. Each frame consists of three columns connected by three horizontal beams.

The dimensions of the structural parts were chosen to fulfil the static design criteria, according to Eurocode, for both the light-weight wooden reference building and the heavy-weight concrete reference building (for details about the static design see Appendix A). The light-weight building consisted of glulam columns and beams and slabs of cross-laminated timber (CLT). The heavy-weight building was made of solid concrete columns, beams and slabs. The cross-sectional dimensions of the structural parts can be seen in Table 6.1. Standard dimensions where used for the glulam columns, beams and CLT slab. The foundation of the reference building consisted of a 200 mm thick concrete slab on soil.
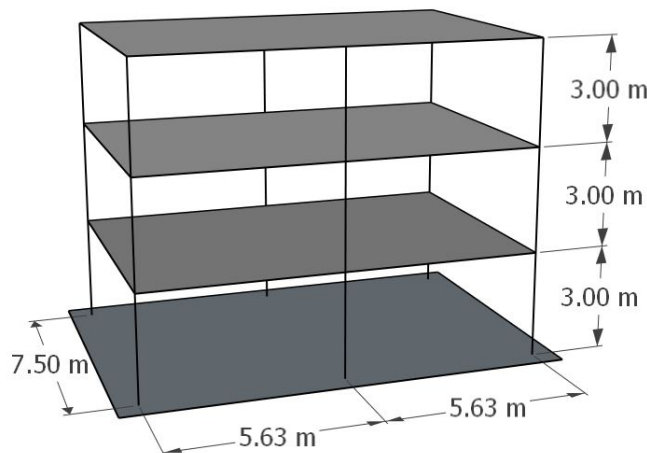
Figure 6.1: *Geometry of the reference building used in the parameter study.*

Table 6.1: *Dimensions of the structural parts in the reference buildings.*

Part	Heavy-weight building	Light-weight building
Column	0.2×0.2 m^2	0.16×0.16 m^2
Beam	0.2×0.4 m^2	0.115×0.36 m^2
Slab thickness	0.3 m	0.28 m (7 layers, 40 mm)

6.1.1   Finite element model

The concrete was modelled as isotropic and the wood as orthotropic and the material parameters are shown in Table 6.2. For the CLT slabs, a composite layup was used which consisted of 7 layers positioned in a cross-wise pattern. The top and bottom layer were positioned with the stiffer axis in the same direction as the slab span-length and the layers between was altered. The individual layers where made of solid wood.

The columns and beams were modelled using 2-node linear beam elements (denoted B31 in Abaqus) and the slabs with 4-node shell elements with reduced integration (denoted S4R in Abaqus). The size of the beam elements was 0.2 m and the shell elements 0.25×0.25 m^2. Rotational and translational tie constraints were used between the beams and slabs. Tie constraints were also used between the columns and the foundation slab, in Abaqus it is known as the *node-to-surface* approach.

The analysis procedure developed in the thesis requires that the connecting surfaces between the ground model and structure model have matching meshes. Thus, the concrete foundation slab was modelled with 20-node 3D quadratic brick elements with reduced integration (denoted C3D20R in Abaqus) with an element size of 1.25×1.25×0.2 m^3. The mesh is shown in Figure 6.2.

Table 6.2: *The parameters of the concrete and wood material [16].*

(a) *Isotropic material parameters of the concrete used in the structure model.*

Material	Concrete
Density [kg/m^3]	2500
Young's Modulus [MPa]	32 000
Poission's ratio [-]	0.2
Loss factor [-]	0.04

(b) *Orthotropic material parameters of the wood used in the structure model.*

Material	Timber
Density [kg/m^3]	500
Loss factor [-]	0.06
E_1 [MPa]	8500
E_2 [MPa]	350
E_3 [MPa]	350
v_{12} [$-$]	0.2
v_{13} [$-$]	0.2
v_{23} [$-$]	0.3
G_{12} [MPa]	700
G_{13} [MPa]	700
G_{23} [MPa]	50
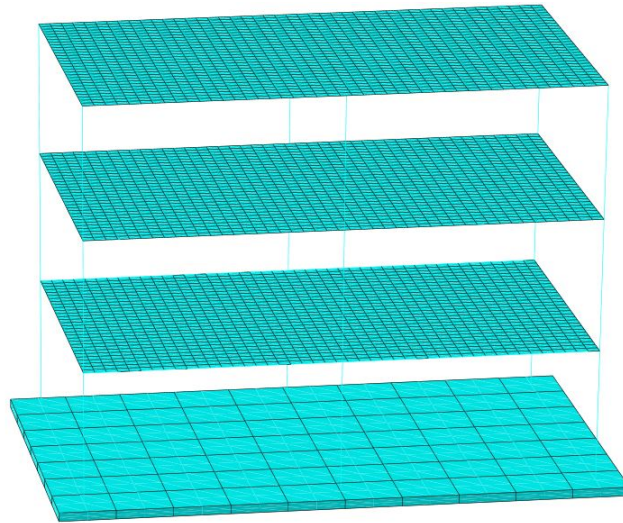
Figure 6.2: *FE mesh of the reference building.*

6.2 Parameter study

Steady-state analyses were performed with a model consisting of a building model coupled to the reduced ground model, as described in Section 4.3. The analyses were conducted over the frequency range 5–50 Hz with 1 Hz steps and with a harmonic vertical unit load applied 20 m from the long side of the building. The placement of the applied load is shown in Figure 6.3. At each frequency, the complex velocity amplitude in both the vertical and horizontal direction were obtained. RMS values of the velocities at all the nodes of the floors were calculated, as in Equation 3.20, and are presented in plots (An example of such plot, see Figure 6.4). RMS values for all the frequencies combined were also calculated, as in Equation 3.21, for each design choice and are presented in tables (An example of such table, see Table 6.3).

Eigenfrequency analysis of the different building models were performed in Abaqus. These analyses were conducted in order to get a estimation of the buildings natural frequencies and to compare these with the peak responses from the parameter study. Seven parameters were altered and the resulting effect was evaluated:

- **Weight**. The heavy-weight building was compared to the light-weight building.

- **Slab span**. The length of the slab span was altered.

- **Slab size**. Both the length of the long side and the length of the short side of the building was altered. The quota between the two lengths was kept constant.

- **Angle of incidence.** The building was rotated around its vertical axis.

- **Slab thickness.** The thickness of the slabs was altered. In the light-weight building both the thickness of each CLT layer and adding additional layers were altered.

- **Column cross-section**. The size of the column cross-section was altered.

- **Beam cross-section**. The size of the beam cross-section was altered.
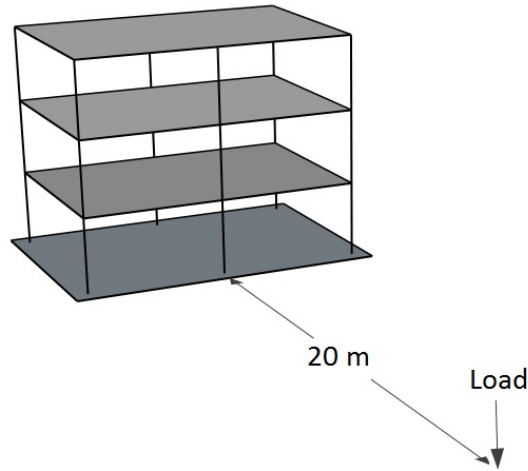
Figure 6.3: *The harmonic load was applied 20 m from the centre of the building's longside.*

6.2.1   Light-weight vs heavy-weight building

The light-weight reference building was compared to the heavy-weight reference building. The response of each floor, the roof and the ground are shown in Figure 6.4 and Figure 6.5.

The ground response is similar for both buildings. Although, a small difference can be seen by comparing the ground response in Figure 6.4a and Figure 6.4b, most notably at 15 Hz. This indicates that the ground response decreases if a heavy-weight building is used. However, the difference is small and at some frequencies, for instance 45 Hz, the weight of the building seems to have a negligible effect on the ground response. In Figure 6.5 it is seen that the horizontal response of both buildings are small compared to the horizontal response of the ground. The study of the column thickness, see Section 6.2.6, indicates that the horizontal movements of the slabs depends on the bending stiffness of the columns. Stiffer columns seems to transfer more horizontal movements from the ground to the slabs.

The peak response of the heavy-weight building is larger than the response of the light-weight building. The total RMS values, seen in Table 6.3, is also larger for the concrete building. In part, this may be explained by the greater material damping applied in the wood building. Also, the light-weight building's eigenmodes that coincided with the large response frequencies of the ground were of higher order than the eigenmodes of the heavy-weight building. An eigenmode with higher order has more complex bending and twisting of the floor slabs, which indicates that more energy may be needed to oscillate these modes.

In Figure 6.4 it is seen that the vibration levels in the buildings are, at some frequencies, greater than the ground response. This indicates that traffic-induced ground vibrations can be amplified in buildings.
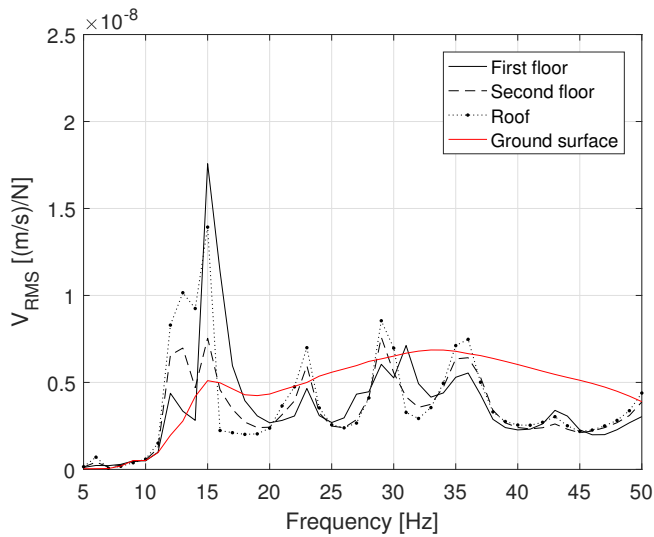
(a) *Light-weight building.*
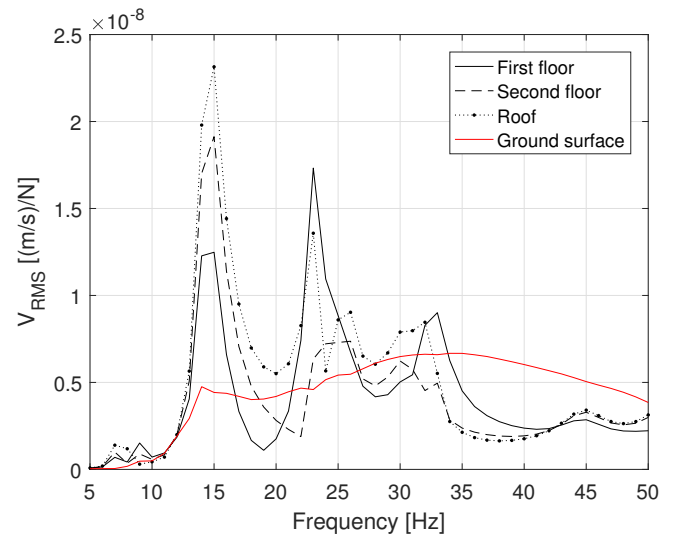
(b) *Heavy-weight building.*

Figure 6.4: *RMS value of the vertical velocity magnitude is presented. At all nodes of the slabs in the light-weight and the heavy-weight building and all nodes in the soil surface below the building.*
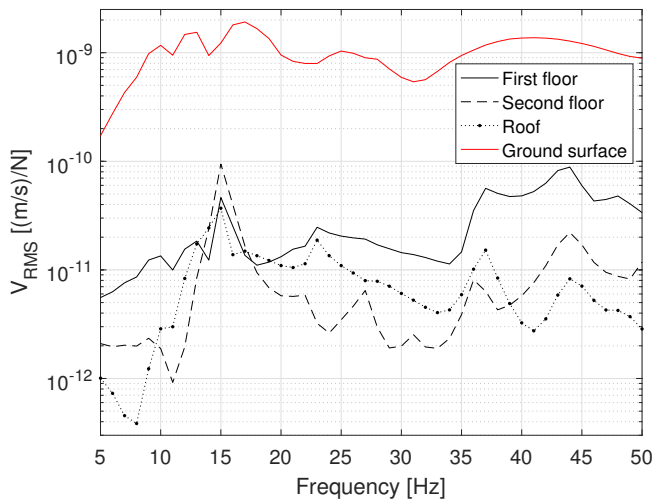
(a) *Light-weight building.*
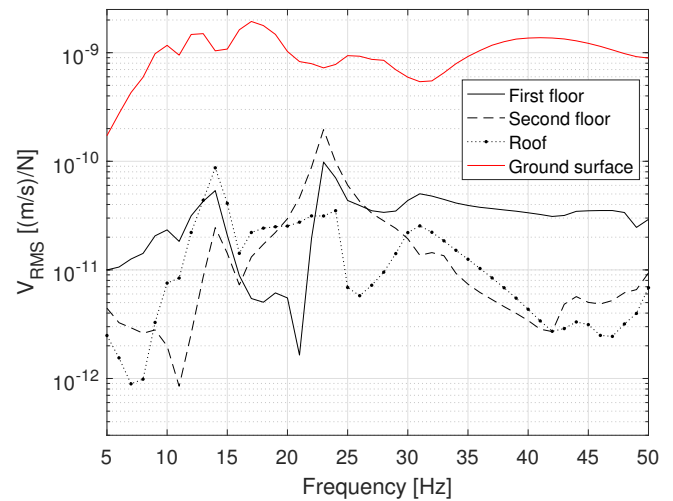
(b) *Heavy-weight building.*

Figure 6.5: *RMS value of the horizontal velocity magnitude is presented with a logarithmic y-axis. At all nodes of the slabs in the light-weight and the heavy-weight building and all nodes in the soil surface below the building. Note the small response of the buildings compare to the response of the ground.*

Table 6.3: *RMS values (5–50 Hz) of the vertical and horizontal velocity magnitude in the light-weight and heavy-weight building.*

Building type	Vertical [10^{-9} (m/s)/N]			Horizontal [10^{-9} (m/s)/N]		
	First floor	Second floor	Roof	First floor	Second floor	Roof
Light-weight	4.64	3.88	4.73	$3.44 \cdot 10^{-2}$	$1.73 \cdot 10^{-2}$	$1.07 \cdot 10^{-2}$
Heavy-weight	5.57	5.56	7.09	$3.58 \cdot 10^{-2}$	$3.91 \cdot 10^{-2}$	$2.16 \cdot 10^{-2}$

6.2.2   Footprint – slab span

The length of the slab span, marked as a red x in Figure 6.6, were altered. For both the light-weight building and the heavy-weight building a longer span resulted in a decrease of the overall RMS values of the vertical vibration levels, shown in Table 6.4. In part this might be explained by the shift of the buildings eigenfrequencies when changing the length of the slab span. Shorter span led to more correlation between the buildings' eigenfrequencies and the large response frequencies of the ground than longer spans.

Also the buildings natural sway frequency is of importance. For instance, when the length of the surface wave is twice the length of the slab span the building is more prone to sway, with one side of the building being pushed up by the wave crest and the other side being pulled down by the wave trough. This could be amplified by the natural sway frequencies of the building. The peak responses in Figure 6.7 and Figure 6.8 in the frequency range of 14–17 Hz all correspond to eigenmode shapes that are prone to sway. However, the eigenmodes of the shorter span correlate more with the large response frequencies of the ground, which might explain the larger response of the buildings with shorter spans.
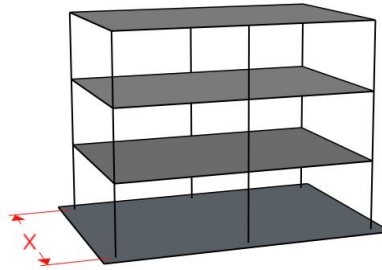
Figure 6.6: *The length of the slab span, that was altered, is marked with a red* x.

(a) *First floor.*   **(b)** *Second floor.*
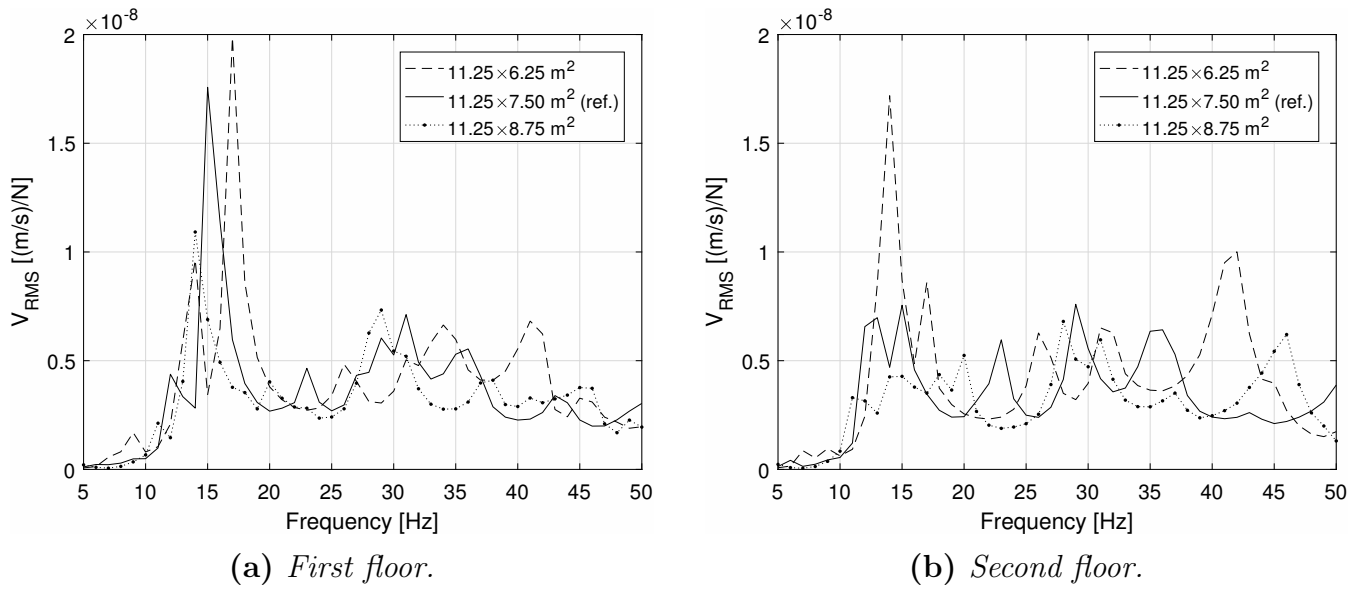
Figure 6.7: *The response of the light-weight building. The length of the slab span was altered. RMS value of the vertical velocity magnitude at all nodes of the floors is presented.*

(a) *First floor.*   **(b)** *Second floor.*
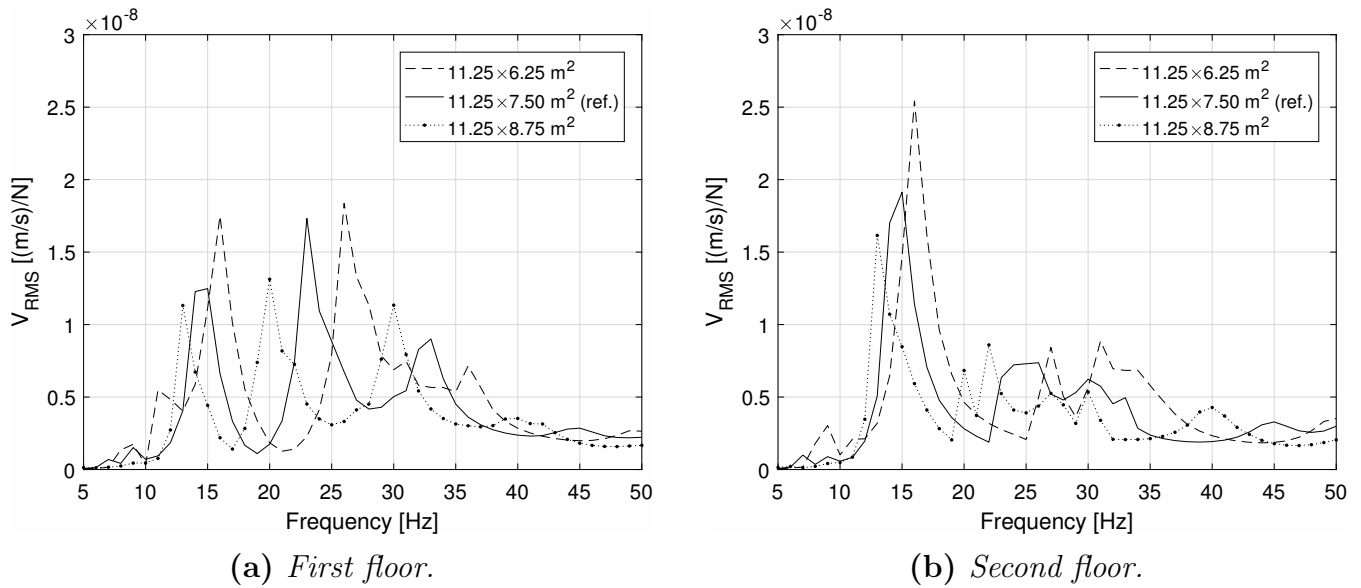
Figure 6.8: *The response of the heavy-weight building. The length of the slab span was altered. RMS value of the vertical velocity magnitude at all nodes of the floors is presented.*

Table 6.4: *RMS values (5–50 Hz) of the vertical and horizontal velocity magnitude in the light-weight and the heavy-weight building. The length of the slab span was altered.*

Slab span length [m]	Vertical [10^{-9} (m/s)/N]		Horizontal [10^{-9} (m/s)/N]	
	First Floor	Second floor	First Floor	Second floor
6.25	5.16	5.23	$5.85 \cdot 10^{-2}$	$1.47 \cdot 10^{-2}$
7.50 (ref.)	4.64	3.88	$3.44 \cdot 10^{-2}$	$1.73 \cdot 10^{-2}$
8.75	3.79	3.48	$2.72 \cdot 10^{-2}$	$1.34 \cdot 10^{-2}$

(a) *Light-weight building.*

Slab span length [m]	Vertical [10^{-9} (m/s)/N]		Horizontal [10^{-9} (m/s)/N]	
	First Floor	Second floor	First Floor	Second floor
6.25	6.40	6.49	$5.58 \cdot 10^{-2}$	$3.36 \cdot 10^{-2}$
7.50 (ref.)	5.57	5.56	$3.58 \cdot 10^{-2}$	$3.91 \cdot 10^{-2}$
8.75	4.82	4.57	$3.59 \cdot 10^{-2}$	$4.26 \cdot 10^{-2}$

(b) *Heavy-weight building.*

6.2.3   Footprint – slab size

The slab size of the building was altered but the quota between the length of the long side and short side of the building was kept constant. Because of the soil-structure mesh requirement a foundation slab of 15×15 m^2 was used. If a foundation slab of the same size as the floor slabs were to be used, both the quota and the mesh requirement could not be maintained.

The RMS values of the vibration, in Table 6.5, for both the light-weight and the heavy-weight building are decreasing with larger slab size, except for the vertical magnitude of the second floor in the light-weight reference building. The response decrease may be explained by the change of the eigenfrequencies in the building, which occurred by altering the slab size. A larger slab size resulted in eigenfrequencies that did not coincide with the large response frequencies of the ground as much as the eigenfrequencies of a smaller slab size. In addition, the eigenmodes that did coincide were, for the building with larger slab sizes, of higher order and thus more energy may be needed to oscillate these modes. Further, the longer span length may be less coinciding with the lengths of the incoming surface waves, which means that the eigenmodes for the larger slab size buildings are not as easily excited.
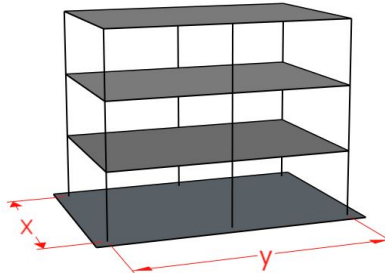
Figure 6.9: *The short side and the long side on the building are marked with a red* x *and* y, *respectively. The Slab size was altered so that the quota between* x *and* y *was the same.*

(a) *First floor.*   (b) *Second floor.*
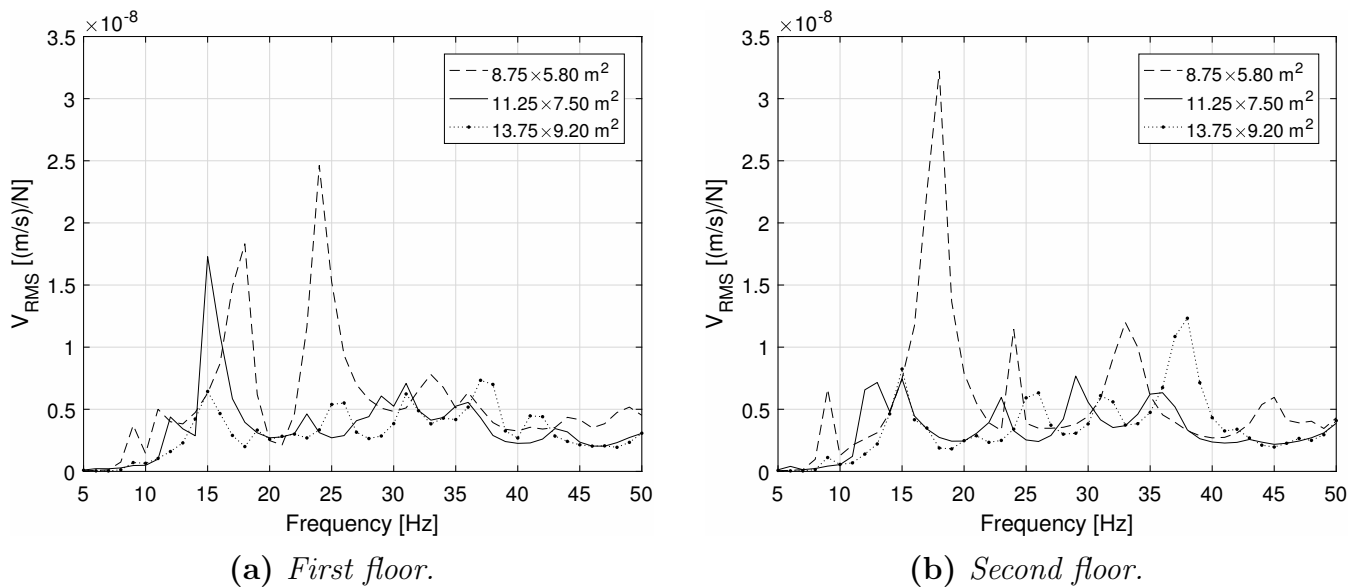
Figure 6.10: *The response of the light-weight building. The slab size of the building was altered but the quota between the length of the short side and the long side of the building was constant. RMS value of the vertical velocity magnitude at all nodes of the floors is presented.*

(a) *First floor.*   (b) *Second floor.*
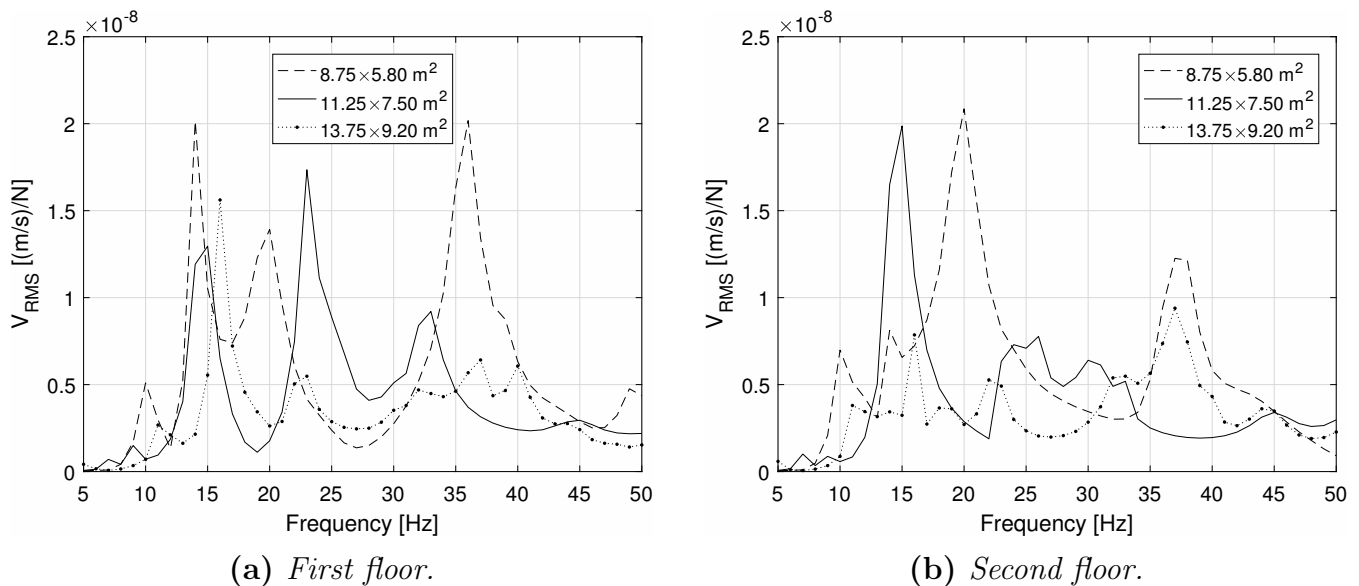
Figure 6.11: *The response of the heavy-weight building. The slab size of the building was altered but the quota between the length of the short side and the long side of the building was constant. RMS value of the vertical velocity magnitude at all nodes of the floors is presented.*

Table 6.5: *RMS values (5–50 Hz) of the vertical and horizontal velocity magnitude in the light-weight and the heavy-weight building. The slab size of the building was altered but the quota between the length of the short side and the long side of the building was constant.*

Slab size [m^2]	Vertical [10^{-9} (m/s)/N]		Horizontal [10^{-9} (m/s)/N]	
	First Floor	Second floor	First Floor	Second floor
8.75×5.80	7.38	8.06	$4.85 \cdot 10^{-2}$	$2.30 \cdot 10^{-2}$
11.25×7.50 (ref.)	4.59	3.87	$2.93 \cdot 10^{-2}$	$1.66 \cdot 10^{-2}$
13.75×9.20	3.61	4.37	$2.76 \cdot 10^{-2}$	$0.713 \cdot 10^{-2}$

(a) *Light-weight building.*

Slab size [m^2]	Vertical [10^{-9} (m/s)/N]		Horizontal [10^{-9} (m/s)/N]	
	First Floor	Second floor	First Floor	Second floor
8.75×5.8	7.66	7.33	$7.63 \cdot 10^{-2}$	$5.32 \cdot 10^{-2}$
11.25×7.5 (ref.)	5.62	5.63	$3.27 \cdot 10^{-2}$	$3.92 \cdot 10^{-2}$
13.75×9.2	4.22	3.93	$2.76 \cdot 10^{-2}$	$3.53 \cdot 10^{-2}$

(b) *Heavy-weight building.*

6.2.4   Rotation of building

The effect by rotating the building around its vertical axis was investigated. As reference, the building was placed with the long side facing the load and the different angles of rotation were 22.5, 45, 67.5 and 90 degrees. Rotation by 90 degrees is equivalent to place the building with the short side facing the load. In Figure 6.12, a rotation of the building is shown. As the nodes of the mesh of the foundation slab were required to correlate to the nodes of the reduced ground model mesh (as explained in Section 4.3), a larger foundation slab was used to be able to rotate the building. The larger foundation slab was 15×15×0.2 m^3 and was not rotated together with the building.

The buildings position relative the incoming ground surface waves seems to effect which eigenmodes that are excited. Comparing the peak responses in Figure 6.13 and Figure 6.14 with the eigenfrequency analysis of the building indicated that different eigenmodes were dominating the response at different rotation angles.
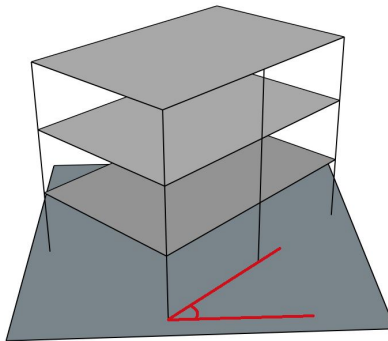
Figure 6.12: *The building is rotated with an angle, marked in red, around its vertical axis.*

In Table 6.6b, the total RMS values for the heavy-weight building is shown. A trend of lower RMS values for both horizontal vibration and vertical vibration can be seen when the rotation angle is increased. This indicates that placing the heavy-weight building with the short side facing the source of vibration will decrease the vibration levels. However, no such trend could be seen for the light-weight building in Table 6.6a.

(a) *First floor.*   (b) *Second floor.*
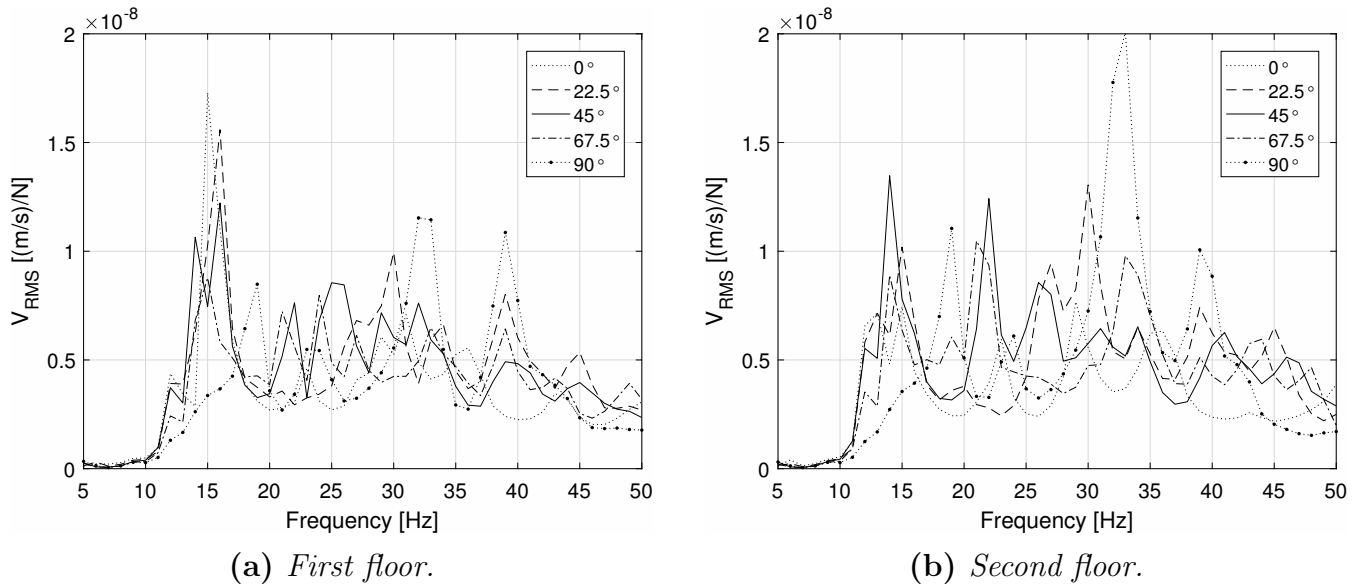
Figure 6.13: *The response of the light-weight building. Rotating the building around its vertical axis. Rotation by 0° places the buildings long side facing the load. RMS value of the vertical velocity magnitude at all nodes of the floors is presented.*

(a) *First floor.*   (b) *Second floor.*
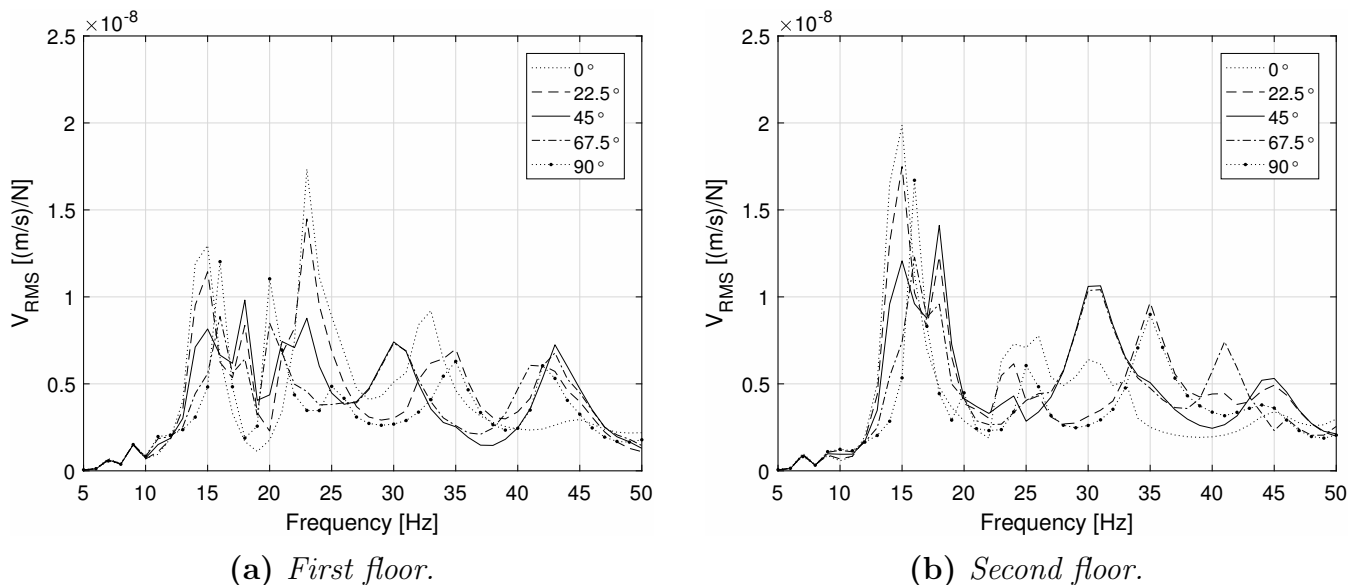
Figure 6.14: *The response of the heavy-weight building. Rotating the building around its vertical axis. Rotation by 0° places the buildings long side facing the load. RMS value of the vertical velocity magnitude at all nodes of the floors is presented.*

Table 6.6: *RMS values (5–50 Hz) of the vertical and horizontal velocity magnitude in the light-weight and the heavy-weight building. Rotating the building around its vertical axis. Rotation by 0° places the buildings long side facing the load.*

Angle of rotation	Vertical [10^{-9} (m/s)/N]		Horizontal [10^{-9} (m/s)/N]	
	First Floor	Second floor	First Floor	Second floor
0°	4.59	3.87	$2.93 \cdot 10^{-2}$	$1.66 \cdot 10^{-2}$
22.5°	5.32	5.45	$6.56 \cdot 10^{-2}$	$2.49 \cdot 10^{-2}$
45°	5.10	5.43	$5.33 \cdot 10^{-2}$	$2.97 \cdot 10^{-2}$
67.5°	4.43	5.09	$4.80 \cdot 10^{-2}$	$1.79 \cdot 10^{-2}$
90°	4.82	6.36	$4.08 \cdot 10^{-2}$	$0.887 \cdot 10^{-2}$

(a) *Light-weight building.*

Angle of rotation	Vertical [10^{-9} (m/s)/N]		Horizontal [10^{-9} (m/s)/N]	
	First Floor	Second floor	First Floor	Second floor
0°	5.62	5.63	$3.27 \cdot 10^{-2}$	$3.92 \cdot 10^{-2}$
22.5°	5.32	5.79	$2.93 \cdot 10^{-2}$	$3.39 \cdot 10^{-2}$
45°	4.73	5.66	$2.66 \cdot 10^{-2}$	$2.47 \cdot 10^{-2}$
67.5°	4.46	5.26	$4.53 \cdot 10^{-2}$	$2.31 \cdot 10^{-2}$
90°	4.15	4.54	$2.23 \cdot 10^{-2}$	$0.91 \cdot 10^{-2}$

(b) *Heavy-weight building.*

6.2.5   Slab thickness

The thickness of the slabs, marked as red in Figure 6.15, was varied. In the light-weight building, the number of layers and the layer thickness in the CLT slabs were changed. In the heavy-weight building, the thickness of the concrete slabs was altered.
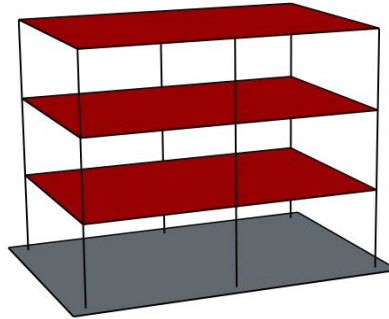
Figure 6.15: *The thickness of the slabs was altered. The slabs are coloured in red.*

Number of layers in the CLT slabs

The effect of altering the number of layers in the CLT slabs of the light-weight building was studied. In Table 6.7, it is seen that the horizontal vibration magnitude decreases in both the first and the second floor using a larger number of layers. In the first floor, the horizontal response decreases by 26% and 53% adding two and four layers, respectively. In the second floor, the horizontal response decreases by 20% and 65% adding two and four layers, respectively.

However, no such trend is seen for the vertical vibration magnitude in Table 6.7. In the first floor, the response increases with a larger number of layers and in the second floor, no strict trend is seen even if the slab with the least layers shows the largest response.

(a) *First floor.*   **(b)** *Second floor.*
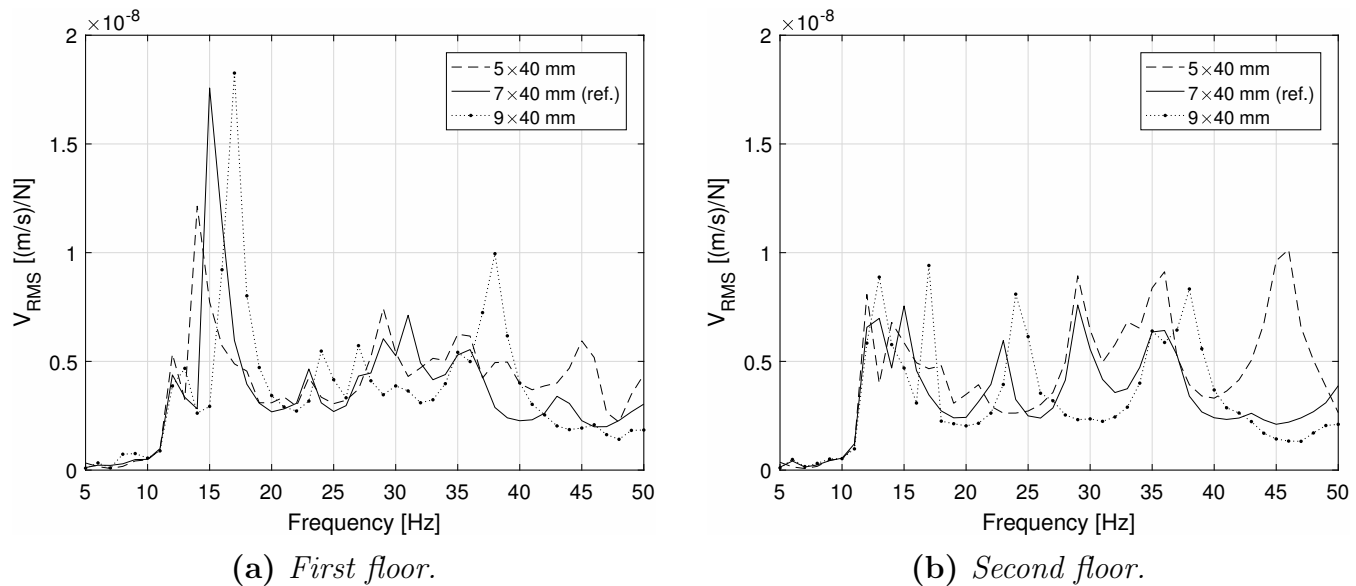
Figure 6.16: *The response of the light-weight building. The number of layers in the CLT slabs was altered. RMS value of vertical velocity magnitude at all nodes of the floors in the light-weight building.*

Table 6.7: *RMS values (5–50 Hz) of the vertical and horizontal velocity magnitude in the light-weight building. The number of layers in the CLT slabs was altered.*

Slab composite	Vertical [10^{-9} (m/s)/N]		Horizontal [10^{-9} (m/s)/N]	
layer layup	First Floor	Second floor	First Floor	Second floor
5×40 mm	4.58	5.15	$4.62 \cdot 10^{-2}$	$2.17 \cdot 10^{-2}$
7×40 mm (ref.)	4.64	3.88	$3.44 \cdot 10^{-2}$	$1.73 \cdot 10^{-2}$
9×40 mm	4.85	4.06	$2.19 \cdot 10^{-2}$	$0.761 \cdot 10^{-2}$

Thickness of layers in the CLT slabs

The effect of altering the layer thickness in the CLT slabs of the light-weight building was studied. In Table 6.7, it is seen that the horizontal vibration magnitude decreases in both the first and the second floor using a thicker slab layers. In the first floor, the horizontal response decreases by 20% and 36% increasing the thickness by 10mm and 20mm, respectively. In the second floor, the horizontal response decreases by 40% and 74% increasing the thickness by 10mm and 20mm, respectively.

However, no such trend is seen for the vertical vibration magnitude in Table 6.7. In the first floor, the response increases with thicker layers and in the second floor, no strict trend is seen. Although, the vertical response in the second floor is largest for the slab made by the thinner layers.

(a) *First floor.*   (b) *Second floor.*
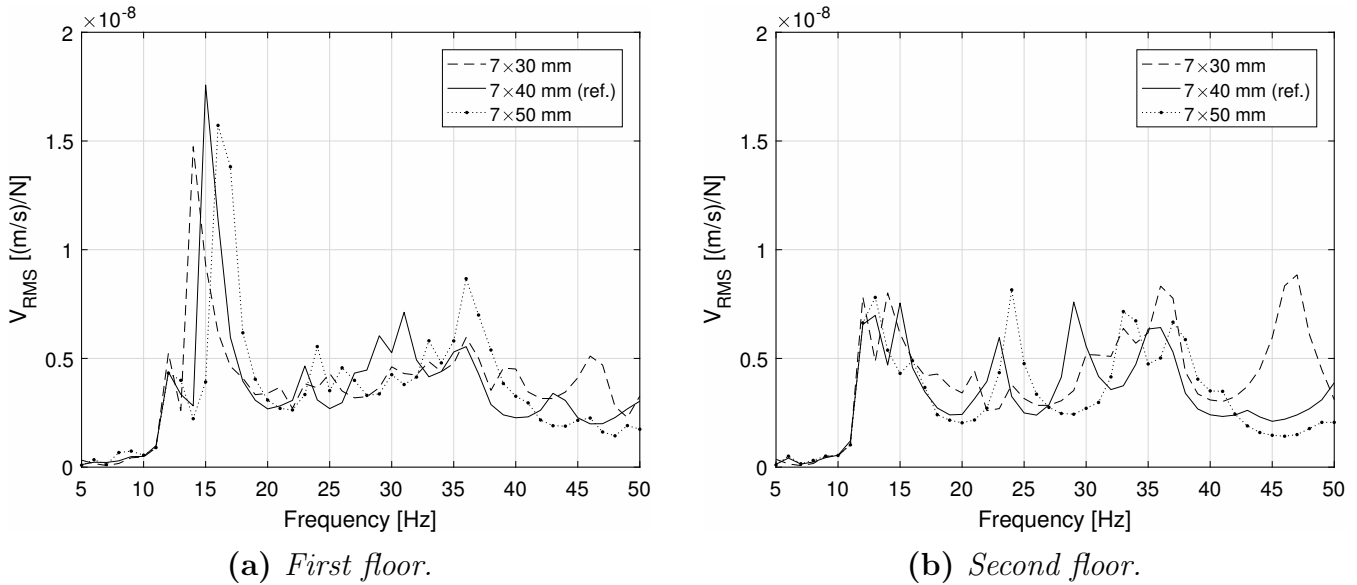
Figure 6.17: *The response of the light-weight building. The thickness of the layers in the CLT slabs was altered. RMS value of vertical velocity magnitude at all nodes of the floors is presented.*

Table 6.8: *RMS values (5–50 Hz) of the vertical and horizontal velocity magnitude in the light-weight building. The thickness of the layers in the CLT slabs was altered.*

Slab composite	Vertical [10^{-9} (m/s)/N]		Horizontal [10^{-9} (m/s)/N]	
layer layup	First Floor	Second floor	First Floor	Second floor
7×30 mm	4.48	4.74	$4.28 \cdot 10^{-2}$	$2.88 \cdot 10^{-2}$
7×40 mm (ref.)	4.64	3.88	$3.44 \cdot 10^{-2}$	$1.73 \cdot 10^{-2}$
7×50 mm	4.77	3.86	$2.37 \cdot 10^{-2}$	$0.750 \cdot 10^{-2}$

Concrete slab thickness

The effect of altering the thickness of the concrete slabs in the heavy-weight building was studied. The RMS values in Table 6.9 indicates that the horizontal response of the slabs were more effected by the change in slab thickness than the vertical response. No significant increase or decrease of the vertical vibration level of the slabs where obtained by changing the slab thickness. For the heavy-weight building the total vertical RMS value only decreased with 10% for the first floor and 16% for the second floor when the thickness of the slabs were changed from 200 mm to 400 mm. It's not realistic to increase each slab's thickness with 100% only to obtain such small reduction in the vibration levels.

(a) *First floor.*   (b) *Second floor.*
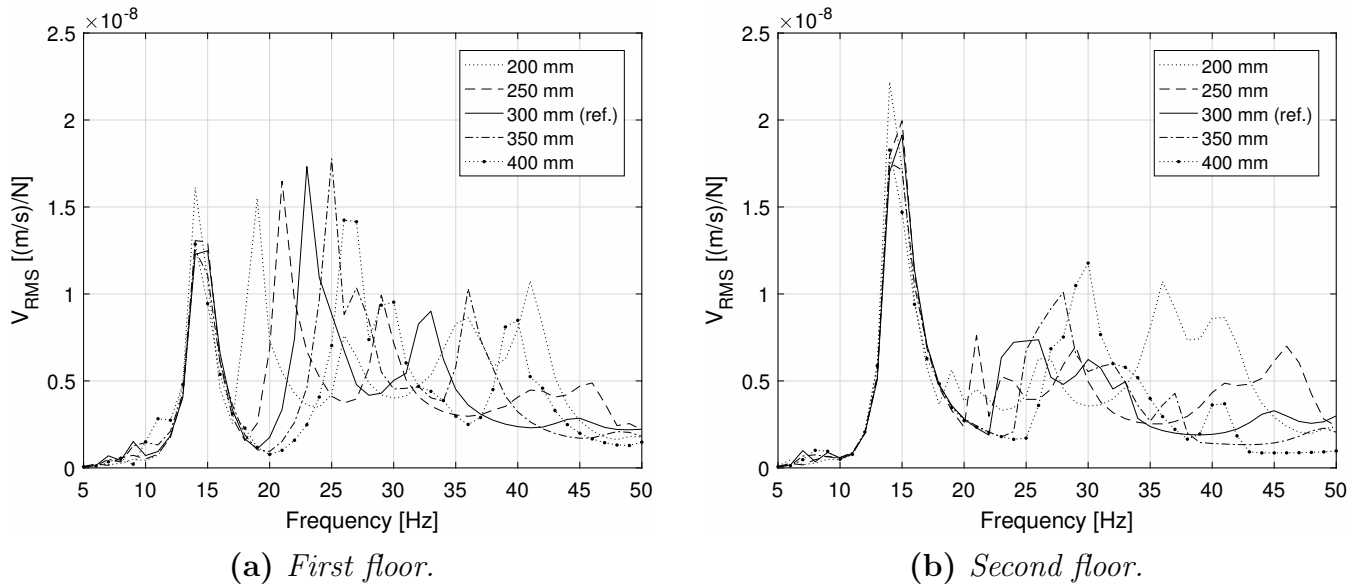
Figure 6.18: *The response of the heavy-weight building. The thickness of the slabs was altered. RMS value of vertical velocity magnitude at all nodes of the floors is presented.*

Table 6.9: *RMS values (5–50 Hz) of the vertical and horizontal velocity magnitude in the heavy-weight building. The thickness of the slabs was altered.*

Slab thickness	Vertical $[10^{-9}$ (m/s)/N]		Horizontal $[10^{-9}$ (m/s)/N]	
	First Floor	Second floor	First Floor	Second floor
200 mm	6.15	6.50	$9.40 \cdot 10^{-2}$	$8.90 \cdot 10^{-2}$
250 mm	5.54	5.88	$5.28 \cdot 10^{-2}$	$5.56 \cdot 10^{-2}$
300 mm (ref.)	5.57	5.56	$3.58 \cdot 10^{-2}$	$3.91 \cdot 10^{-2}$
350 mm	5.67	5.53	$3.05 \cdot 10^{-2}$	$2.85 \cdot 10^{-2}$
400 mm	5.53	5.46	$2.92 \cdot 10^{-2}$	$2.07 \cdot 10^{-2}$

6.2.6   Column cross-section

The effect of altering the size of the column cross-sections was studied, where the columns are coloured red in Figure 6.19. In the light-weight building the cross-sections were chosen according to standard dimensions for glulam columns.

In the eigenfrequency analysis of the building, it could be seen that a larger cross-section of the columns results in higher eigenfrequencies. The peak responses in Figure 6.20 and Figure 6.21 are shifted in frequency according to the increased eigenfrequencies.

According to the values in Table 6.10, larger vibrations occur at the increase of the column cross-section. This may be explained by the increased stiffness of the thicker columns and therefore the increased ability to transfer vibrations to the slabs.
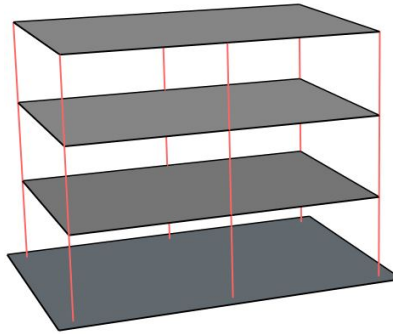
Figure 6.19: *The size of the column cross-section was altered. The columns are coloured red.*

(a) *First floor.*   **(b)** *Second floor.*
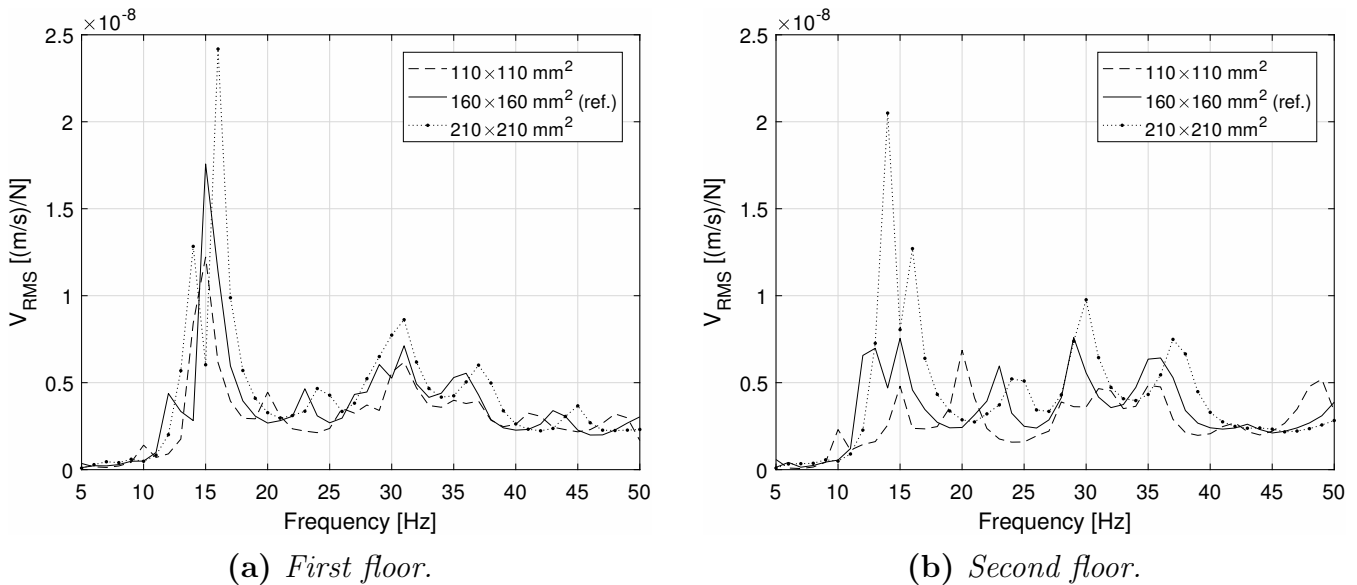
Figure 6.20: *The response of the light-weight building. The size of the column cross-section was altered. RMS value of the vertical velocity magnitude at all nodes of the floors is presented.*

(a) *First floor.*

(b) *Second floor.*
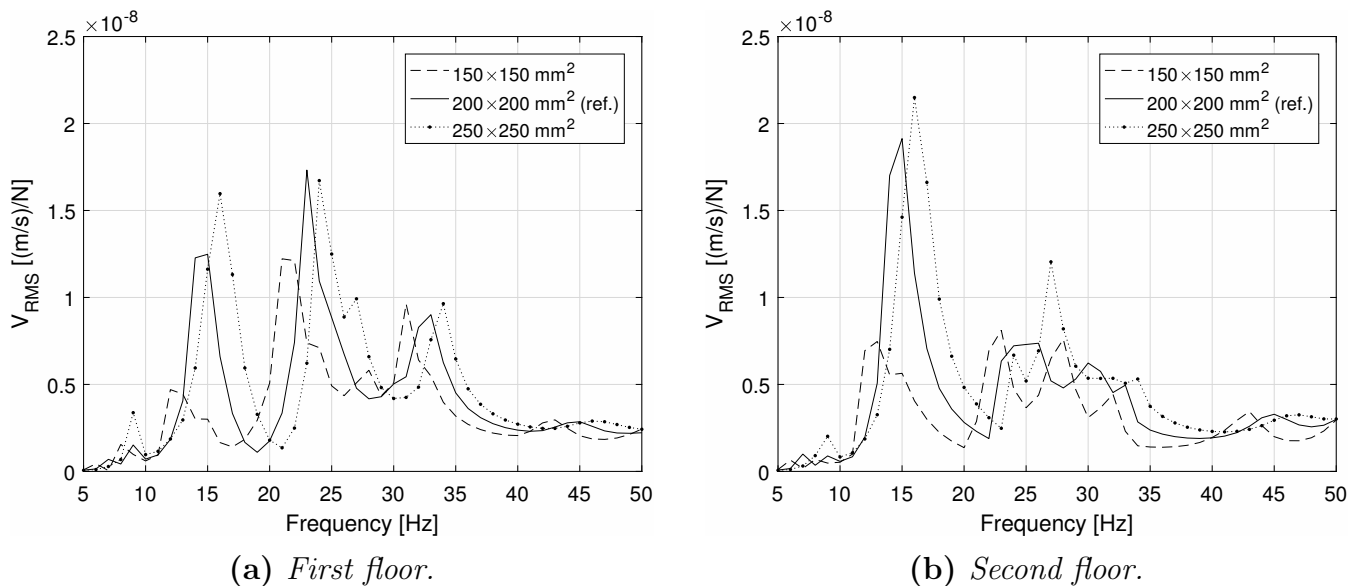
Figure 6.21: *The response of the heavy-weight building. The size of the column cross-section was altered. RMS value of the vertical velocity magnitude at all nodes of the floors is presented.*

Table 6.10: *RMS values (5–50 Hz) of the vertical and horizontal velocity magnitude in the light-weight and heavy-weight building. The size of the column cross-section was altered.*

Glulam column cross-section [mm^2]	Vertical [10^{-9} (m/s)/N]		Horizontal [10^{-9} (m/s)/N]	
	First Floor	Second floor	First Floor	Second floor
110×110	3.76	3.10	$1.46 \cdot 10^{-2}$	$0.63 \cdot 10^{-2}$
160×160 (ref.)	4.64	3.88	$3.44 \cdot 10^{-2}$	$1.73 \cdot 10^{-2}$
210×210	5.80	5.51	$4.19 \cdot 10^{-2}$	$4.88 \cdot 10^{-2}$

(a) *Light-weight building.*

Concrete column cross-section [mm^2]	Vertical [10^{-9} (m/s)/N]		Horizontal [10^{-9} (m/s)/N]	
	First Floor	Second floor	First Floor	Second floor
150×150	4.49	3.70	$3.79 \cdot 10^{-2}$	$1.24 \cdot 10^{-2}$
200×200 (ref.)	5.57	5.56	$3.58 \cdot 10^{-2}$	$3.91 \cdot 10^{-2}$
250×250	6.15	6.35	$5.80 \cdot 10^{-2}$	$8.59 \cdot 10^{-2}$

(b) *Heavy-weight building.*

6.2.7   Beam cross-section

The effect of altering the size of the beam cross-section was studied, where the beams are coloured red in Figure 6.22, was altered. In the light-weight building the cross-sections were chosen according to standard dimensions for glulam beams.
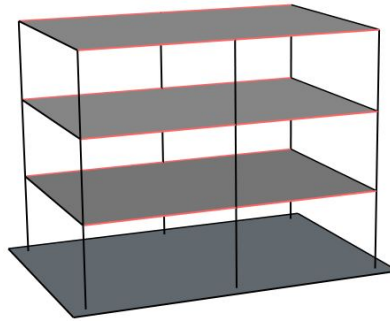
Figure 6.22: *The size of the beam cross-section was altered. The beams are coloured red.*

Compared to altering other parameters, the beam cross-section had the smallest effect on the RMS value of the vertical and horizontal velocity magnitude. This is seen for both the light- and heavy-weight building in Table 6.11.
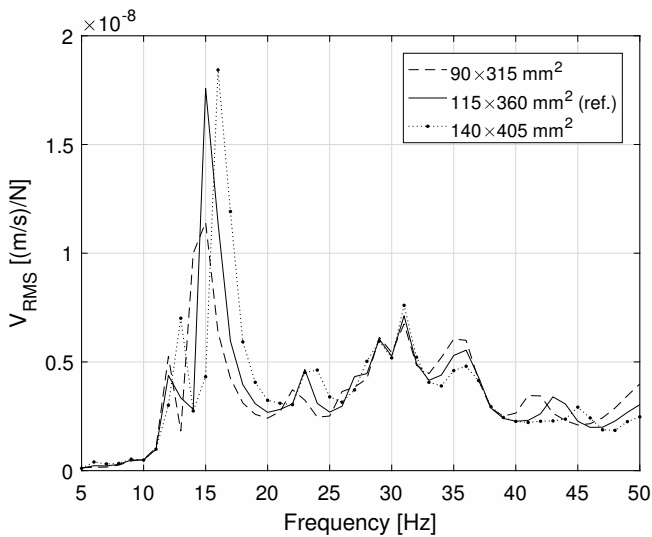
(a) *First floor.*
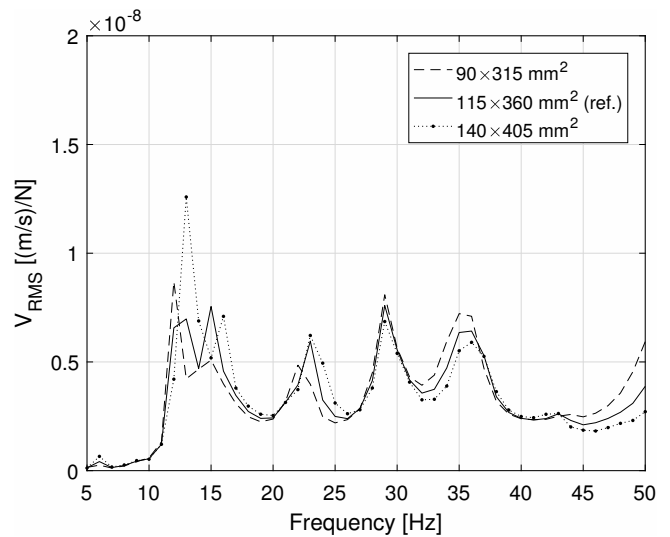
(b) *Second floor.*

Figure 6.23: *The response of the light-weight building. The size of the beam cross-section was altered. The RMS value of the vertical velocity magnitude at all nodes of the floors is presented.*

(a) *First floor.*   (b) *Second floor.*
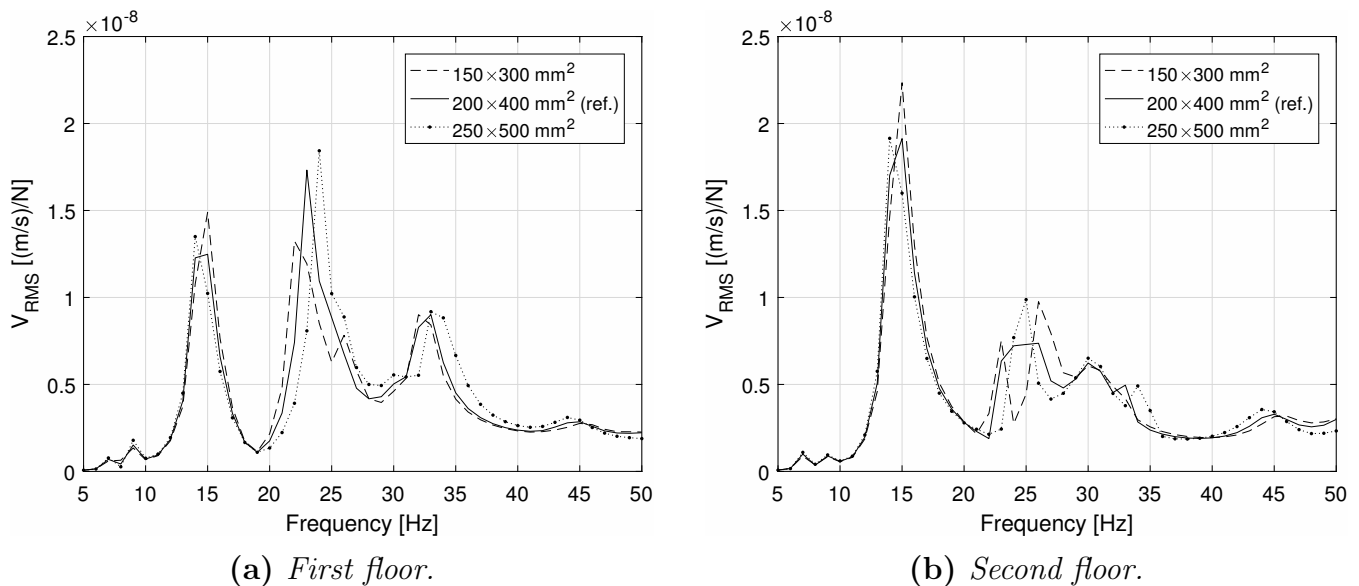
Figure 6.24: *The response of the heavy-weight building. The size of the beam cross-section was altered. The RMS value of the vertical velocity magnitude at all nodes of the floors is presented.*

Table 6.11: *RMS values (5–50 Hz) of the vertical and horizontal velocity magnitude in the light-weight and heavy-weight building. The size of the beam cross-section was altered.*

Glulam beam cross-section [mm^2]	Vertical [10^{-9} (m/s)/N]		Horizontal [10^{-9} (m/s)/N]	
	First Floor	Second floor	First Floor	Second floor
90×315	4.21	3.98	$3.37 \cdot 10^{-2}$	$1.43 \cdot 10^{-2}$
115×360 (ref.)	4.64	3.88	$3.44 \cdot 10^{-2}$	$1.73 \cdot 10^{-2}$
140×405	4.81	4.08	$3.34 \cdot 10^{-2}$	$1.81 \cdot 10^{-2}$

(a) *Light-weight building.*

Concrete beam cross-section [mm^2]	Vertical [10^{-9} (m/s)/N]		Horizontal [10^{-9} (m/s)/N]	
	First Floor	Second floor	First Floor	Second floor
150×300	5.46	5.82	$3.60 \cdot 10^{-2}$	$3.97 \cdot 10^{-2}$
200×400 (ref.)	5.57	5.56	$3.58 \cdot 10^{-2}$	$3.91 \cdot 10^{-2}$
250×500	5.68	5.43	$3.76 \cdot 10^{-2}$	$3.68 \cdot 10^{-2}$

(b) *Heavy-weight building.*

7 Discussion and concluding remarks

7.1 Developed methodology

The main objective of the Master's thesis was to develop an efficient methodology to be used for a parameter study of a building. Therefore was a dynamic condensation method implemented and performed on a ground model in order to obtain a reduced ground model. The developed reduction methodology was simple to implement in the FE software, Abaqus, but it required much available computational resources. This was both due to the large number of dofs in the ground model that was necessary to achieve reliable results, but also the chosen number of retained dofs in the reduced model as this determined the number of load cases. The developed methodology is therefore not feasible if no access to some sort of computational cluster is available. However, after the dynamic condensation, the computation time to perform the steady-state analysis in the parameter study decreased with 99.7% and it could be performed on a regular desktop computer. If many analyses are to be performed with the same ground model, the decreased computation time using the reduced ground model will make it worth the effort and time to perform the dynamic condensation. Although, if only a few analyses with a ground model will be performed it might not be advantageous to perform the dynamic condensation. By establishing several ground models with different ground compositions and with varying soil properties and performing the dynamic condensation on these models, a library of reduced ground models can be created. At a construction site, the ground conditions might match an already reduced ground model in the created library and thus analyses could be performed without the need to establish and perform the dynamic condensation on a new ground model.

No calibrations between the numerical models and experimental results were made because of the comparative nature of the parameter study. However, such calibrations could be implemented in the developed methodology without changing the procedure. No loss of accuracy is introduced by performing the dynamic condensation in the thesis.

At the interface between the reduced ground model and the building model, the two meshes needed to be the same size, i.e. the nodes had to have coinciding coordinates, in order to be connected correctly. This limited how the building's slab foundation was placed and how it was designed. The slab foundation of the building was also connected rigidly to the ground, which is a simplification as the soil-structure interaction is rarely rigid and can provide a mechanism for energy dissipation.

To conclude, some important aspects in the developed methodology are presented.

- The computational time to perform analysis using the reduced model decreases significantly but the dynamic condensation of the ground model can be very computationally costly.

- A larger number of retained dofs in the reduced ground model increases the computational cost for both the dynamic condensation of the ground model and the analysis performed with the reduced ground model.

7.2   Parameter study

The aim of the Master's thesis was to obtain knowledge of building vibrations induced by traffic and the effect structural design might have on these vibrations. Numerical models were used to simulate the propagation of waves and a parameter study, where seven structural design choices of a building were studied. In the parameter study, the vibration level in the slabs of the building were evaluated.

Analysis of vibrations levels in a building is a complicated practice since many factors are involved, which may affect the vibrations. Therefore, it might be difficult to draw conclusions concerning the effect on the vibration level due to specific structural design choices. However, in the result from the numerical simulations it can be seen that structural design can have great effect on the vibrations levels inside a building. To conclude, some important aspects seen in the result of the parameter study are presented.

- A coinciding frequency between the load and the buildings' eigenfrequencies resulted in velocity peak responses in the slabs of the building.

- At a coinciding frequency between the load and a buildings eigenfrequency, the response amplitude in the building depends on the order of the corresponding eigenmode in the building. If the eigenmode was of higher order, the response in the building was lower than if the corresponding eigenmode was of lower order.

- The length of the propagated waves compared to the footprint of the building was important. For example if the length of the footprint is half the length of the propagated wave, this places one side of the building on a crest and the other side on a trough. It may excite a buildings sway mode and result in larger vibration levels in the building.

These trends indicates that knowledge of resonance frequencies for both the surrounding ground and the building are important. In addition, knowledge about the length of the propagating waves could be used in an early design stage in a building process. If both the vibration source and the ground properties at a construction site are known, the length of the propagating wave could be estimated and a footprint size chosen in order to prevent an undesirable match.

7.3   Suggestions for future work

Some suggestions for future work that would be interesting are listed below.

- The reduction of the ground model was very computationally costly, where the approach in which the dynamic condensation was performed have the largest potential to be improved in order to decrease the computational cost of the reduction. Thus, it would be interesting to investigate and find alternative approaches to perform the dynamic condensation. An alternative would be to explore the possibility to use so called iterative solution strategies, which can solve large linear equation systems to a smaller computational cost.

- Implementation of constraints between the reduced FE ground model and the FE building model would be interesting for further studies. That could remove the requirement of matching meshes at the interface.

- The effect on the induced building vibrations due to different foundation, e.g. column foundation, slab foundation and cellar foundation, would be interesting in further studies.

- Uncertainties were introduced at several stages during the analysis, e.g. in the ground model, a soil and bedrock profile were chosen and the material properties of the ground were approximated. In the building model the connections were chosen as tied, this may also be an introduced uncertainty. All uncertainties contributes to a numerical result that deviates more from the actual real-life value. This indicates that instead of presenting a scalar value at each frequency, an interval should be presented. The interval should then contain the sought real-life value and it may be compared to the guidelines. As a future work, it is suggested that these uncertainties are investigated and the interval determined.

Bibliography

[1] United Nations Department of Economic and Social Affairs - Population Division, *World urbanization prospects: The 2014 revision*. New York UN, 2015.

[2] P. Persson, *Vibrations in a built environment: Prediction and Reduction*. PhD thesis, Report TVSM-1026, Lund University, 2016.

[3] N. Persson, *Predicting railway-induced ground vibrations*. Master's thesis, Report TVSM-5212, Lund University, 2016.

[4] V. V. Krylov, A. Dawson, M. Heelis, and A. Collop, "Rail movement and ground waves caused by high-speed trains approaching track-soil critical velocities," *Proceedings of the Institution of Mechanical Engineers, Part F: Journal of Rail and Rapid Transit*, vol. 214, no. 2, pp. 107–116, 2000.

[5] L. Hall and C. Wersäll, *Markvibrationer*, vol. 1. SGF informationsskrift, 2012.

[6] M. Bahrekazemi, *Train-induced ground vibration and its prediction*. PhD thesis, Royal Institute of Technology, Stockholm, 2004.

[7] T.M. Dawn and C.G. Stanworth, "Ground vibrations from passing trains," *Journal of Sound and Vibration*, vol. 66, no. 3, pp. 355–362, 1979.

[8] Statens Naturvårdsverk och SP, *Lathund för omvandling mellan olika vibrationsstorheter*. PM 1993-02-19.

[9] Swedish transport administration (Trafikverket), *Störs du av vibrationer från trafiken?* http://www.trafikverket.se/resa-och-trafik/trafikbuller-och-vibrationer/vad-gor-trafikverket-at-buller-och-vibrationer/Stors-du-av-vibrationer-fran-trafiken/. Accessed: 2017-04-13.

[10] L. Andersen, *Linear elastodynamic analysis*. Aalborg University. Department of Civil Engineering, 2006.

[11] N. S. Ottosen and H. Petersson, *Introduction to the finite element method*. Prentice-Hall, 1992.

[12] J. Lysmer and R. L. Kuhlemeyer, "Finite dynamic model for infinite media," *Journal of the Engineering Mechanics Division*, vol. 95, no. 4, pp. 859–878, 1969.

[13] Dassault Systèmes, *Abaqus 6.14 Documentation*. 2014.

[14] A. K. Chopra, *Dynamics of structures*, vol. 3. Prentice Hall, New Jersey, 1995.

[15] H. Bodén, *Ljud och vibrationer*. Royal Institute of Technology, Stockholm, 2011.

[16] O. Flodén, *Vibration transmission in lightweight buildings -Numerical prediction models*. PhD thesis, Report TVSM-1028, Lund University, 2014.

[17] Mathworks, *Matlab 2016 Users Guide*, vol. 2016.

[18] Lunarc, *Computer cluster Aurora*. Center for scientific and technical computing at Lund University, 2017.

[19] T. A. Davis, *UMFPACK Version 4.0 User Guide*. University of Florida, 2002.

[20] T. A. Davis, *Direct methods for sparse linear systems*. SIAM, 2006.

[21] J. R. Gilbert, C. Moler, and R. Schreiber, "Sparse matrices in Matlab: Design and implementation," *SIAM Journal on Matrix Analysis and Applications*, vol. 13, no. 1, pp. 333–356, 1992.

[22] Rydén, Tyréns, NGI, and Peab, *MaxLab IV - Geodynamic parameters for the ground*. Norwegian Geodynamic Institute, 2011.

A Static design of the reference buildings

The buildings were statically designed in the failure limit state according to Eurocode load case STR B 6.10b. It was chosen to be a residence building and located in Lund. The characteristic values for the snow and wind load for this location can be seen in Table A.1.

In the design of the building, hinged connections and simply supported columns, beams and slabs were assumed. Security class 3 has been chosen. A stabilising system of the building was taken into account during the static design of the columns, beams and slabs. Although, the stabilising system has not been designed and not accounted for in the parameter study.

Table A.1: *The characteristic ground snow load (s_k) and the reference wind velocity (v_b) according to Eurocode in Lund Kommun. The assumed terrain type at the reference building.*

s_k	1.5 kN/m^2
v_b	26 m/s
Terrain type	III

A.1 Heavy-weight building

The heavy-weight building consists of beams, columns and solid slabs in concrete. The parameters of the chosen concrete can be seen in Table A.2. The reinforcement used in the structure can be seen in Table A.3.

Table A.2: *The quality, the characteristic compressive strength (f_{ck}) and the density of the concrete.*

	Quality	f_{ck} [MPa]	Density [kg/m^3]
Concrete	C30	30	2500

Table A.3: *The type, the diameter, the design yield strength (f_{yd}) and the Young's modulus of the reinforcement bars.*

	Type	Diameter [mm]	f_{yd} [MPa]	Young's modulus[MPa]
Reinforcement bars	B500BT	16	435	200 000

The beams were chosen to have a rectangular cross-section and as they were assumed to be simply supported, the cross-section was dimensioned for the field moment at half the span with reinforcement in the lower part in the cross-section. The cross-section of the columns were chosen to be square and the reinforcement was places symmetrically. The concrete slab was designed by studying product sheets of several manufacturers and taking an overall estimate of the thickness of the slab. The cross-section of the beams, the columns and the slabs in the heavy-weight reference building can be seen in Table A.4.

Table A.4: *The dimension of the beams, columns and slabs in the heavy-weight reference building.*

	Width [mm]	Height [mm]	Length [mm]
Beam	200	400	5625
Column	200	200	3000
Slab	7500	300	11 250

A.2   Light-weight building

The light-weight building represents a wooden building consisting of columns and beams in glulam and a slab made of CLT (Cross-Laminated Timber). The properties of the glulam can be seen in Table A.5. CLT is constructed by gluing together laminates of timber, which can be in the quality of construction timber, where the direction of the fibers in one layer is orthogonal to the closest layer but parallel to the second closest layer. The top and bottom layers have parallel fibers in the direction of the span, i.e. CLT has an odd number of layers.

Table A.5: *The quality, the characteristic bending strength (f_{mk}), the characteristic compression strength parallel to fibers (f_{ck}), the Young's modulus and the density of the Glulam.*

	Quality	f_{mk} [MPa]	f_{ck} [MPa]	Young's modulus [MPa]	Density [kg/m^3]
Glulam	GL32h	32	29	11 000	450

The dimensions of the beams and columns were chosen according to standard dimensions found at glulam manufacturers, which also sufficed in the failure limit state. The CLT slabs were designed by studying the product sheet of manufactures. The cross-section of the beams, the columns and the slabs in the light-weight reference building can be seen in Table A.6.

Table A.6: *The dimension of the beams, columns and slabs in the light-weight reference building.*

	Width [mm]	Height [mm]	Length [mm]
Beam	115	360	5625
Column	160	160	3000
Slab	7500	280 (7 layers)	11 250